Model Order Reduction Methods for Topology Optimization

Erik ten Hagen

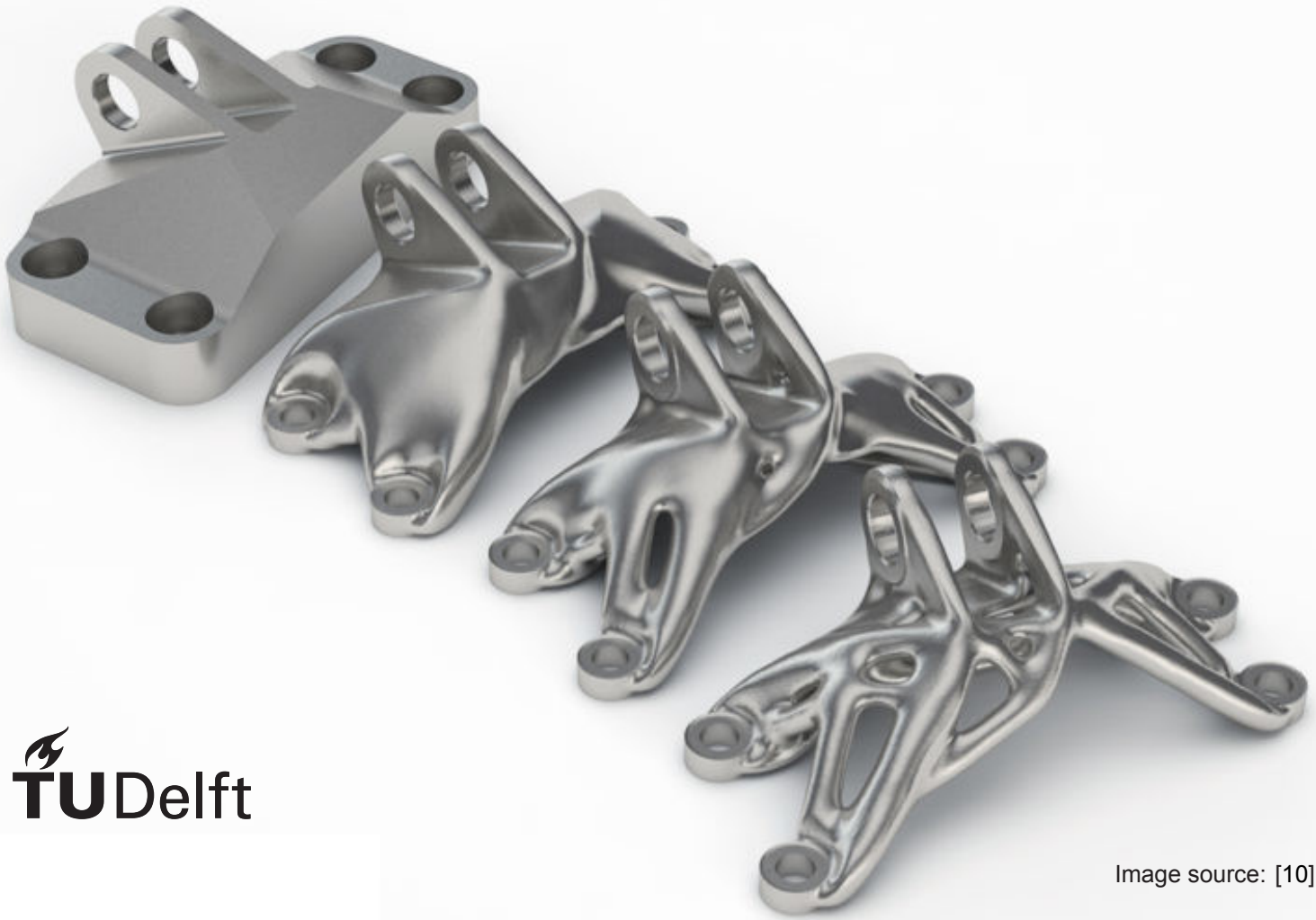

TU Delft

Image source: [10]

Model Order Reduction Methods for Topology Optimization

by

Erik ten Hagen

to obtain the degree of Master of Science
at the Delft University of Technology,
to be defended publicly on Tuesday August 30, 2022 at 2:00 PM.

Student number:	4477944	
Project duration:	April 1, 2021 – August 30, 2022	
Thesis committee:	Prof. dr. ir. M. van Gijzen,	TU Delft, supervisor
	Prof. dr. ir. A. W. Heemink,	TU Delft
	Dr. ir. M. Langelaar,	TU Delft

TU Delft

Abstract

Topology optimization is a branch of mechanical engineering in which the topology of a structure is created and optimized to certain conditions and restrictions. In the last few decades, the demand for highly accurate and complex models of these structures has increased and it has a big effect on the computational power needed. To ease the computational load for the dynamical systems one can use model order reduction methods to reduce the size of the models. Classic Arnoldi is a widely used method for model order reduction (MOR) with topology optimization. In this thesis, we discuss two-sided Arnoldi and IRKA to help find a suitable moment-matching MOR method for topology optimization. These two reduction methods are implemented and improved to create a high fidelity reduced model. For improvements in the accuracy, the use of orthogonalization methods is analysed and discussed as well as including rigid body modes for IRKA and a preconditioner for two-sided Arnoldi. Lastly, a participation factor is discussed and improved to help reduce the model created with two-sided Arnoldi. In the end, we find that two-sided Arnoldi in combination with the participation factor performs better than IRKA by creating a smaller and more accurate reduced model.

Preface

One of the key aspects I enjoy in mathematics is the ease in which it is combined with other fields, ranging from modelling the trajectory of electrons in an electron scanner to modelling the propagation of water in a tsunami wave to finding lost items drifting at sea. With this interest in mind, I choose a topic where the numerical analysis of mathematics faces real-world problems.

I am grateful for the countless talks and discussions I had with Martin van Gijzen. This made my research both educational and gratifying. I would also like to thank Arnoud Delissen, a PhD candidate working on topology optimization who helped me understand some of the physics involved and provided an example to evaluate the methods discussed in this thesis.

Erik ten Hagen
Boskoop, August 2022

Contents

List of Figures

List of Tables

1 Introduction

Topology optimization is a branch of mechanical engineering in which the topology of a structure is created and optimized to certain conditions and restrictions. Applications can range from bookshelf brackets to equipment in high-tech industries. Especially for the bigger/critical structures, you want to have a model of the structure as accurately as possible. This requires a very fine mesh of the domain used with the finite element method to solve differential equations. Only, this can get very expensive to calculate. The computational cost for topology optimization can be reduced with the use of Model Order Reduction (MOR) for it reduces the size of the model. There is a large variety of MOR methods to help us reduce the size of a model. In this thesis, the category moment matching is discussed. Reduced models created with moment matching approximate the full model around one or multiple interpolation points. The interpolation points play a crucial role in where the reduced model is accurate.

The main research question for this thesis is

What is a suitable moment matching MOR method for topology optimization?

Before this question can be answered we should know

How to choose the interpolation points for moment matching MOR?

and

How to choose the size of the reduced-order system?

In the category moment matching, there are still a large number of methods to choose from. In this thesis, the focus will lie on a variant of Arnoldi and IRKA. Arnoldi is chosen for it is extensively described in the literature and often used. The variant that will be discussed is two-sided Arnoldi and is an extension of the original algorithm. IRKA is chosen to evaluate since it can iteratively determine the 'optimal' location of the interpolation points. To help determine the size of a reduced-order system a participation factor will be introduced for Arnoldi. This participation factor calculates how much influence certain vectors have and vectors with a small influence can be discarded, which will reduce the size of the reduced model created with Arnoldi.

The thesis is structured by first introducing the methods of topology optimization, model order reduction and the participation factor. Then various improvements are suggested for IRKA, two-sided Arnoldi and the participation factor. These improvements will then be evaluated on two examples, of which one is a topology optimization example. Lastly, the methods will be evaluated on benchmark problems created for model order reduction.

2

Methods

To properly show the results of this report an introduction is required on several topics. Therefore, this chapter is dedicated to the introduction of the three subjects. First topology optimization to get a grasp on the situations where the reduction methods can be used. Then model order reduction will be explained and some of its methods. Shortly, different orthogonalization methods are disccused and lastly, the participation factor will be introduced, this factor is used to improve one of the model order reduction methods.

2.1. Topology Optimization

In this section, topology optimization will be introduced as well as its relationship to LTI systems which later on will be used for model order reduction. Also, some of the mathematical properties of these systems will be shown.

2.1.1. What is Topology Optimization?

Topology optimization is a broad subject and is used for different applications. It tries to find the 'best' structure given some user-defined load, conditions and constraints. How 'best' is defined depends on the problem, it can vary from maximizing the load capacity of a structure to minimizing resonance or material in a structure. These goals can be used as constraints as well. For example, maximizing the load capacity of a structure while only using a certain amount of the material. Sometimes the structure has to fulfill some conditions. For example when the structure needs to be bolted to another object it needs material for the bolts to hold onto. At the same time there might be some areas of the structure where no material is allowed, because the area is already occupied by other structures. A large class of dynamical systems is described by the following matrix equation

$$\begin{aligned} M\ddot{x} + D\dot{x} + Kx &= bu \\ y &= c^T x \end{aligned} \tag{2.1}$$

where M, D and K are the mass, dampening and stiffness matrix respectively. u is the actuator/input, y is the sensor/output and x is the state of the system. The systems discussed in this report all assume that M is invertible.

The topology optimization algorithm is applied to a discretized domain where it starts with an initial guess. In every iteration it moves material until it creates the 'best' structure and every node ends with having the value one or zero corresponding to having material or having no material. Since in every iteration the material moves, the stiffness (and mass) matrix changes and therefore a linear system of equations has to be solved multiple times. These operations can get very expensive.

2.1.2. Example of Topology Optimization

A popular topology optimization example is the 99 line Matlab code from O. Sigmund [21] in which topology optimization is used for a Messerschmitt-Bölkow-Blohm (MBB) beam. This is a classic structural design problem of a symmetric beam with a downward directed load in the middle and has supports on

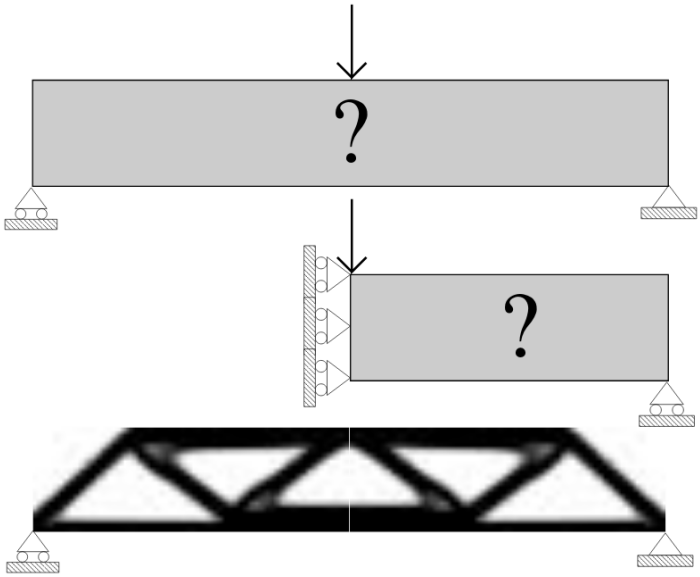

Figure 2.1: The design domain and full domain of an MBB beam which is a classical example for topology optimization [21].

both sides. The objective for topology optimization here is to minimize the compliance with a constraint on the amount of material used. In Figure 2.1 the design area of the full domain and half domain is shown. For this example, the stiffness matrix is calculated and $Kx = b$ is solved in every iteration. The evolution of the topology is shown in Figure 2.2.

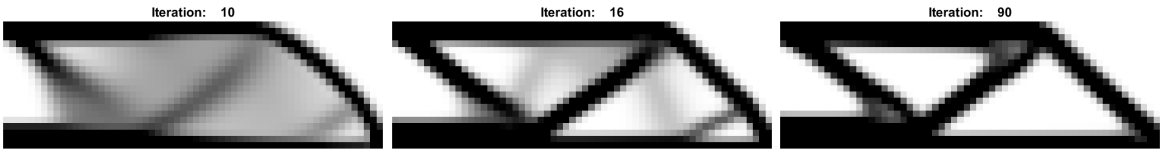

(a) Iteration 10 (b) Iteration 16 (c) Iteration 90

Figure 2.2: The optimization process within different stages showing iteration 10, 16 and 90.

2.1.3. The Equations used for MOR Methods

The focus of this thesis lies in topology optimization for more complex systems, which use actuators and sensors. The MOR methods that we will consider are for first-order systems. The second-order system will therefore first be reduced to a first-order by introducing an auxiliary variable $z = \dot{x}$ [4, 17, 18]. Substituting this in the first line of Equation (2.1) results in

$$M\dot{z} = -Dz - Kx + bu(t) \tag{2.2}$$

$$\dot{x} = z \tag{2.3}$$

The full first-order system becomes

$$\begin{bmatrix} M & 0 \\ 0 & I \end{bmatrix} \begin{bmatrix} \dot{z} \\ \dot{x} \end{bmatrix} = \begin{bmatrix} -D & -K \\ I & 0 \end{bmatrix} \begin{bmatrix} z \\ x \end{bmatrix} + \begin{bmatrix} b \\ 0 \end{bmatrix} u(t)$$
$$y = \begin{bmatrix} 0 \\ c \end{bmatrix}^T \begin{bmatrix} z \\ x \end{bmatrix} \tag{2.4}$$

Now the model order reduction methods can be used for this first-order linear time-invariant (LTI) system used in topology optimization.

2.1.4. Natural Frequencies of the System

A natural frequency or eigenfrequency of a system is a frequency at which the system resonates naturally, which means without external interference or input. For many applications you want to know what the natural frequencies are, since resonance caused by natural frequencies can jeopardise a structures integrity. Therefore avoiding resonance in a certain frequency band is sometimes used as one of the constraints for topology optimization.

To find the eigenfrequencies of a system we have to mention eigenvalues and eigenmodes and how these three relate to each other. To find the eigenvalues and eigenmodes of a second-order system a solution has to be found for the homogeneous linear equation

$$M\ddot{x} + D\dot{x} + Kx = 0. \tag{2.5}$$

The general solution is of the form $x(t) = \tilde{x}e^{\lambda t}$ with a constant eigenvector or eigenmode $\tilde{x}$ and eigenvalue λ [6].

The homogeneous equation can be rewritten with the general solution to

$$(\lambda^2 M + \lambda D + K)\tilde{x} = 0 \tag{2.6}$$

This is known as the quadratic eigenvalue problem. For systems with n degrees of freedom it has $2n$ solutions, which are real or in conjugate pairs. Suppose $\lambda = \alpha + i\beta$ then the solution can be written as

$$x(t) = \tilde{x}e^{\alpha t}(\cos(\beta t) + i\sin(\beta t))$$

The real part of the eigenvalue of the solution determines the decay of the corresponding eigenmode over time and the imaginary part describes the rate of oscillation of that eigenmode. The eigenfrequency of the system is $\omega = \beta$ [16, 22]. For systems without dampening all the eigenvalues are purely imaginary [14].

For the first-order homogeneous linear equation

$$E\dot{x} = Ax \tag{2.7}$$

with

$$E = \begin{bmatrix} M & 0 \\ 0 & I \end{bmatrix} \qquad \text{and} \qquad A = \begin{bmatrix} -D & -K \\ I & 0 \end{bmatrix}$$

the eigenvalue problem is

$$Av = \lambda Ev$$

The eigenvalues and modes can be easily calculated when they are already known for the second-order system of Equation (2.4). They are calculated as

$$\begin{aligned} (A - \lambda E)v &= 0 \\ \begin{bmatrix} -D - \lambda M & -K \\ I & -\lambda I \end{bmatrix} \begin{bmatrix} v_1 \\ v_2 \end{bmatrix} &= 0 \\ -Dv_1 - \lambda M v_1 - Kv_2 &= 0 \\ v_1 &= \lambda v_2 \\ \lambda D v_2 + \lambda^2 M v_2 + K v_2 &= 0 \end{aligned}$$

thus the eigenvalues of the first-order linear system are the same as the eigenvalues of the polynomial eigenvalue problem of Equation (2.6).

2.1.5. LTI Systems

LTI systems are systems that are linear and time-invariant. First, a linear system is a system where the result of taking a linear combination of the inputs is the same as the linear combination of the result of each of the individual inputs. Second, time-invariant systems are systems which always give the same output given the same input independent of when in time it happens. These systems are recognizable when the matrices do not depend on time. The first order LTI system is

$$\begin{aligned} E\dot{x}(t) &= Ax(t) + bu(t) \\ y(t) &= c^T x(t) \end{aligned} \tag{2.8}$$

in which u,y and x are the input, output and state variables respectively. To get a direct relation between the input and the output a Laplace transformation is applied to the three variables. The Laplace transformation is defined by

$$\mathcal{L}\{f(t)\} = \int_0^\infty e^{-st} f(t) dt \tag{2.9}$$

The Laplace transformed variables are $U(s), Y(s)$ and $X(s)$. The system can now be written as

$$\begin{aligned} Y(s) &= H(s)U(s) \\ H(s) &= c^T(sE - A)^{-1}b \end{aligned} \tag{2.10}$$

where $H(s)$ is called the transfer function of the system and is the relation between the input and the output of the system.

2.2. Model Order Reduction

A large variety of physical phenomena are modelled with linear time-invariant systems. These systems are getting increasingly complex and bigger, due to more detailed modelling of the underlying physical problem. These developments require more and more computational power. One of the methods to alleviate this computational load is called Model Order Reduction (MOR). This reduces the size of the problem and therefore decreases the computational power needed to solve the system. There is a range of different methods to reduce the order of a model. In this report only moment matching methods are discussed.

2.2.1. Theory

MOR methods are used to reduce a system of size n to size r with $r << n$. The methods create a V, W of size $n \times r$ where $x \approx V x_r$ and the reduced model is

$$\begin{aligned} E_r \dot{x}_r(t) &= A_r x_r(t) + b_r u(t) \\ y_r(t) &= c_r^T x_r(t) \end{aligned} \tag{2.11}$$

with

$$A_r = W^* A V \qquad E_r = W^* E V$$
$$b_r = W^* b \qquad c_r = cV$$

Often W is chosen to be the same as V for simplicity of the reduction.

One category of methods that reduces the order of models is called moment matching. This method evaluates the transfer function by making a Taylor expansion of $H(s)$ around one or multiple interpolation points $s_i \in \mathbb{C}$, which are not a pole of $H(s)$. To demonstrate how to rewrite the transfer function we use one interpolation point s_0.

The transfer function is

$$H(s) = -c^T(A - s_0 E - (s - s_0)E)^{-1}b \tag{2.12}$$

For ease of notation we define

$$\beta = -(A - s_0 E)^{-1} b \qquad \text{and} \qquad G = (A - s_0 E)^{-1} E$$

In the steps of rewriting the transfer function we use the properties of a Neumann series. When a Neumann series converges then the following property holds

$$(I - T)^{-1} = \sum_{k=0}^{\infty} T^k$$

The transfer function can now be written as

$$H(s) = -c^T(A - s_0E - (s - s_0)E)^{-1}b \tag{2.13}$$
$$= -c^T(I - (A - s_0E)^{-1}(s - s_0)E)^{-1}(A - s_0E)^{-1}b \tag{2.14}$$
$$= c^T(I - (s - s_0)G)^{-1}\beta \tag{2.15}$$
$$= \sum_{k=0}^{\infty} c^T G^k \beta (s - s_0)^k \tag{2.16}$$
$$H(s) = c^T\beta + c^T G\beta(s - s_0) + c^T G^2\beta(s - s_0)^2 + \dots \tag{2.17}$$
$$H(s) = \mu_0 + \mu_1(s - s_0) + \mu_2(s - s_0)^2 + \dots \tag{2.18}$$

with $\mu_i = c^T G^i \beta$ are the moments of the transfer function. Further information can be found in [4]. The moment matching methods create a V (and W) by matching the first k moments in the reduced transfer function $H_r(s)$ with the moments of $H(s)$:

$$H(s) = H_r(s) + \mathcal{O}((s - s_0)^k). \tag{2.19}$$

The more moments you match the better the approximation of the reduced system becomes. The moments of the transfer function can be calculated explicitly

$$\text{with } \mu_j = c^T G^j \beta \text{ or with } \mu_{2j} = ((G^T)^j c)^T (G^j \beta) \text{ and } \mu_{2j+1} = ((G^T)^j c)^T (G^{j+1}\beta).$$

The explicit calculations of the moments should be avoided since it is an extremely ill-conditioned problem [4, 9]. The moments can also be calculated implicitly which is done with the use of Krylov subspaces. A Krylov subspace is defined for a matrix N and vector q and the subspace is the span of the vector q and the multiple multiplications of q with the matrix N. This subspace is denoted as

$$\mathcal{K}_r(N, q) = \text{span}\{q, Nq, N^2q, \dots, N^{r-1}q\}. \tag{2.20}$$

If only the right-sided Krylov subspace $\mathcal{K}_r(G, \beta)$ is used in a MOR method then r moments are matched and W is chosen to be the same as V. When the left-sided Krylov space $\mathcal{K}_r(G^T, c)$ is used it can match up to $2r$ moments. How the matrix and vector in the Krylov space are chosen depends on the location of the interpolation point(s). There are three possibilities. The interpolation point is in 0, in σ or in ∞. The right-sided Krylov subspaces for these three interpolation points are respectively

$$\mathcal{K}_r(A^{-1}E, A^{-1}b), \quad \mathcal{K}_r((A - \sigma E)^{-1}E, (A - \sigma E)^{-1}b) \quad \text{and} \quad \mathcal{K}_r(E^{-1}A, E^{-1}b).$$

The left-sided Krylov subspaces for the three interpolation points are respectively

$$\mathcal{K}_r(E^*A^{-*}, c), \quad \mathcal{K}_r(E^*(A - \sigma E)^{-*}, c) \quad \text{and} \quad \mathcal{K}_r(A^*E^{-*}, c) \text{[4, 9].}$$

Since the focus of this report lies on matching the transfer function around the smallest eigenvalues we focus on the interpolation point σ using the Krylov subspaces $\mathcal{K}_r((A - \sigma E)^{-1}E, (A - \sigma E)^{-1}b)$ and $\mathcal{K}_r(E^*(A - \sigma E)^{-*}, c)$. This is often called the shift-and-inverted Krylov subspaces.

In this report two different moment matching methods will be discussed and compared. The first method is Arnoldi and its variant two-sided Arnoldi, which matches r and $2r$ moments respectively. The second method is called IRKA, a relatively new method for model order reduction that uses r interpolation points to create a V and W and matches two moments at each interpolation point.

2.2.2. Arnoldi and Two-sided Arnoldi

The Arnoldi method [3] is a widely used method for moment matching model order reduction. When it was first created the method was meant to find the largest eigenvalues of the equation

$$(\lambda I - A)x = 0.$$

This is done by first reducing the order of the system. The Arnoldi method creates a V to be an orthogonal basis of the Krylov subspace with $V^*V = I$. For the reduction of the system one takes $W = V$. The reduced eigenvalue problem can then be written as

$$V^*(\lambda I - A)Vx_r = 0$$
$$(\lambda V^*V - V^*AV)x_r = 0$$

When an eigenvector is a linear combination of the vectors v_i then their corresponding eigenvalue is an eigenvalue of V^*AV. This method can be extended to large unsymmetric generalized eigenproblem [15]

$$Ax = \lambda Ex. \tag{2.21}$$

The process of Arnoldi's method as shown in Algorithm 1 [24] starts with an initial vector for the Krylov subspace q, normalizes the vector and then starts finding the next vector in the Krylov subspace by multiplying it with a matrix N. To retain orthonormality a modified Gram Schmidt orthogonalization is applied before creating the next vector in the Krylov subspace. After k iterations you get a reduced matrix A_r and the orthonormal columns that span the Krylov subspace are in the matrix V. This method can be used for different goals when a different N and q are chosen. For example when we want to use moment matching around a shift we have to choose $N = (A - \sigma E)^{-1}E$ and $q = (A - \sigma E)^{-1}b$. This is called shift-and-invert Arnoldi [15].

The Arnoldi method uses the right-sided Krylov subspace and creates only a V matrix. This means it can match at most r moments of the transfer function. Therefore we want to introduce two-sided Arnoldi. This method creates a right-sided Krylov space V with $\mathcal{K}_r(G, \beta)$ and a left-sided Krylov space W with $\mathcal{K}_r(G^T, c)$ by doing the Arnoldi method twice and can therefore match up to $2r$ moments of the transfer function [19]. The matrices V and W are orthogonalized with themself and not bi-orthogonalized. The method is shown in Algorithm 2. This algorithm can be used for shift-and-invert two-sided Arnoldi when the input is chosen as $\mathbf{A} = (A - \sigma E)^{-1}E$, $\mathbf{b} = (A - \sigma E)^{-1}b$ and $\mathbf{c} = c$. The reduced matrices are calculated with $A_r = W^*AV$ and $E_r = W^*EV$.

Algorithm 1: Arnoldi

Input: A, b, k
Initialize: $r = b$, $\beta = ||r||_2$
for $j = 1...k$ **do**
  $v_j = r/\beta$
  $r = Av_j$
  for $i = 1...j$ **do**
    $h_{ij} = v_i^T r$
    $r = r - h_{ij}v_i$
  $\beta = ||r||_2$
  if $j < k$ **then**
    $h_{j+1,j} = \beta$
$v_k = r/\beta$
Output: $A_r = H[1:k, 1:k]$, $V = [v_1, ..., v_k]$

2.2.3. IRKA

In [13] Gugercin et al introduce an Iterative Rational Krylov Algorithm (IRKA). This is an interpolatory model reduction method that aims to construct an $H_r(s)$ that interpolates $H(s)$ in a set of shifts $\sigma_i \in \mathbb{C}$.

Algorithm 2: Two-sided Arnoldi

Input: A, b, c, k
Initialize: $r = b$, $\beta = ||r||_2$, $s = c$, $\gamma = ||s||_2$
for $j = 1...k$ **do**
  $v_j = r/\beta$
  $w_j = s/\gamma$
  $r = Av_j$
  $s = A^T w_j$
  for $i = 1...j$ **do**
    $h_1 = v_i^T r$
    $h_2 = w_i^T s$
    $r = r - h_1 v_i$
    $s = s - h_2 w_i$
  $\beta = ||r||_2$
  $\gamma = ||s||_2$
$v_k = r/\beta$
$w_k = s/\gamma$
Output: $V = [v_1, ..., v_k]$, $W = [w_1, ..., w_k]$, $A_r = W^* AV$

The shifts have a positive real part and are closed under conjugation and are a Hermite interpolation points such that

$$H(\sigma_i) = H_r(\sigma_i), \qquad H'(\sigma_i) = H_r'(\sigma_i) \qquad \text{for i} = 1...k \tag{2.22}$$

A standard method for judging the accuracy of the approximation of the reduced transfer function is by taking the $\mathcal{H}_2$ norm. The $\mathcal{H}_2$ norm is described for a function $F(s)$ by [27]

$$||F||_2^2 = \frac{1}{2\pi} \int_{-\infty}^{\infty} \text{trace}[F^*(\omega i) F(\omega i)] d\omega \tag{2.23}$$

IRKA aims to find a high fidelity reduced system by minimizing the error $||H - H_r||_2^2$. To achieve this the shifts should be well placed. Antoulas et al. found out that the shifts should be the mirror images of the poles of the reduced-order system [2, 13]. Since these shifts are not known a priori the algorithm finds them iterative. The method is shown in Algorithm 3 [5, 17].

When a certain tolerance is met or when the maximum iteration is reached IRKA constructs a V and W with the latest found σ's such that

$$range(V) = \text{span}\{(\sigma_1 E - A)^{-1} b, ..., (\sigma_k E - A)^{-1} b\} \tag{2.24}$$
$$range(W) = \text{span}\{(\sigma_1 E - A)^{-*} c, ..., (\sigma_k E - A)^{-*} c\} \tag{2.25}$$

The matrices of the reduced system are calculated by $E_r = W^* EV$, $A_r = W^* AV$, $b_r = W^* b$ and $c_r = cV$ [2].

2.3. Orthogonalization Methods

The orthogonality of vectors in a matrix is discussed extensively in this thesis, but has not been formally introduced yet. The standard method of orthogonalization 'transforms' a matrix V such that $V^* V = I$ as is shown in Algorithm 4. It is also possible to transform two matrices such that $W^* V = I$, this is called biorthogonalization and is shown in Algorithm 5. The orthogonalization of matrices can be extended to include a mass matrix, this is called mass-orthogonalization. The idea of mass-orthogonalizing V and W is often seen in physics. The vectors are normalized or orthogonalized with respect to the mass matrix. The effect of this is that parts or particles with a large mass gets prioritized over parts or particles of the system with a relatively small mass. To apply this idea in the first-order system the matrices V and W should be orthogonalized with respect to the matrix E, resulting in $V^* EV = I$ and $W^* EW = I$ or for biorthogonalization $W^* EV$. The algorithms are shown in Algorithm 6 and Algorithm 7.

Algorithm 3: IRKA Algorithm

Input: A,E, b, c, k, tol
Initialize: Select $S_k = \{\sigma_1, ..., \sigma_k\} \in \mathbb{C}$ closed under conjugation
Choose V and W such that
Ran(V) = span $\{(A - \sigma_1 E)^{-1} b, ..., (A - \sigma_k E)^{-1} b\}$,
Ran(W) =span $\{(A - \sigma_1 E)^{-*} c, ..., (A - \sigma_k E)^{-*} c\}$.
while $tol <$ *relative change in* $\{\sigma_i\}$ **do**
    $A_r = W^* AV$, $E_r = W^* EV$
    assign $\sigma_i = -\lambda(A_r, E_r)$
    update V and W such that
    Ran(V) = span$\{(A - \sigma_1 E)^{-1} b, ..., (A - \sigma_k E)^{-1} b\}$ and
    Ran(W) =span$\{(A - \sigma_1 E)^{-*} c, ..., (A - \sigma_k E)^{-*} c\}$.
Output: $A_r = W^* AV$, $b_r = W^* b$, $c_r = cV$, $E_r = W^* EV$

Algorithm 4: Orthogonalisation

Input: V
Initialize: $k = size(V)$
for $j = 1...k$ **do**
    $v = V(:, j)$
    for $i = 1...j - 1$ **do**
        $\alpha = V(:, i)^* v$
        $v = v - \alpha V(:, i)$
    $V(:, j) = v / \sqrt{v^* v}$
Output: V

Algorithm 5: Biorthogonalisation

Input: V,W
Initialize: $k = size(V)$
for $j = 1...k$ **do**
    $v = V(:, j)$
    $w = W(:, j)$
    for $i = 1...j - 1$ **do**
        $\alpha = W(:, i)^* v$
        $\beta = V(:, i)^* w$
        $v = v - \alpha\, V(:, i)$
        $w = w - \beta\, W(:, i)$
    $V(:, j) = v / (w^* v)$
    $W(:, j) = w$
Output: V, W

Algorithm 6: Mass-orthogonalisation

Input: V, E
Initialize: $k = size(V)$
for $j = 1...k$ **do**
    $v = V(:, j)$
    for $i = 1...j - 1$ **do**
        $\alpha = V(:, i)^* E v$
        $v = v - \alpha\, V(:, i)$
    $V(:, j) = v / \sqrt{v^* E v}$
Output: V

Algorithm 7: Mass-Biorthogonalisation

Input: V, W, E
Initialize: $k = size(V)$
for $j = 1...k$ **do**
  $v = V(:, j)$
  $w = W(:, j)$
  for $i = 1...j-1$ **do**
    $\alpha = W(:, i)^* E v$
    $\beta = V(:, i)^* E w$
    $v = v - \alpha V(:, i)$
    $w = w - \beta W(:, i)$
  $V(:, j) = v/(w^* E v)$
  $W(:, j) = w$
Output: V, W

2.4. Participation Factor

With model order reduction a basis is created for the projection of the full system. A difficult task for this is to estimate how big the basis should be. Wilson et al. [25] came up with an idea to help decrease the size of the basis. After creating a basis for the reduced system, each basis vector will be given a value depending on its importance in the original system. When a basis vector has little to no importance to the system it can be removed. The reduced system will be smaller and less computational power is needed to compute the reduced system.

Wilson et al. [25] worked on a dynamic equation for a structural system and with the displacement vector x.

$$M\ddot{x} + D\dot{x} + Kx = b \tag{2.26}$$

For his model order reduction they used a basis V created from the Krylov space $\mathcal{K}_r(K^{-1}M, K^{-1}b)$ with each vector of v being mass-orthogonalized. They did not include damping for their Krylov subspace.

The participation factor for the basis vectors they introduced was

$$p_i = v_i^T b \tag{2.27}$$

with $v_i \in V$. The load vector is described by the finite series

$$b = \sum_j q_j M v_j$$

and since the vectors v are mass-orthogonalized $V^T M V = I$, this $q_j = p_j$. The error for the load vector is defined as

$$e = b - \sum_j p_j M v_j$$

An error norm for the load vector is introduced as

$$\epsilon = \frac{b^T e}{b^T b}.$$

When the reduced model exist of zero vectors then this error norm is one. When the reduced model contains all the vectors of the system then this error norm is zero. Alternatively, the contribution of each basis vector to the load vector can be described by

$$h_i = \frac{b^T p_i M v_i}{b^T b} \tag{2.28}$$

The downside of this method is that it does not take into account the dynamics of a system and is only suitable for low-frequency problems.

Then Gu et al. [12] extended this idea, where they worked on the same matrix equation of the linear structural dynamics of Equation 2.26. To create a reduced system suitable for higher frequency they used a different Krylov space. They used $\mathcal{K}_r((K + i\omega_c D - \omega_c^2 M)^{-1}M, (K + i\omega_c D - \omega_c^2 M)^{-1}b)$ in which ω_c is in the middle of the frequencies of interest. They included this idea also in the participation factor and defined it as

$$p_i = \frac{|v_i^T s|}{[(v_i^T v_i)(s^T s)]^{1/2}} \tag{2.29}$$

$$s = (K + \Omega i D - \Omega^2 M)^{-1} b \tag{2.30}$$

where s is the frequency response at a specific frequency Ω. When there is a system in which multiple frequencies are of interest the following participation factor is suggested

$$p_i = \max_j \frac{|v_i^T s_j|}{[(v_i^T v_i)(s_j^T s_j)]^{1/2}} \tag{2.31}$$

$$s_j = (K + \Omega_j i D - \Omega_j^2 M)^{-1} b \tag{2.32}$$

with Ω_j the different frequencies of interest.

This new participation factor gives a value between 0 and 1. This can be further extended to a participation factor p_{ij} where multiple frequencies Ω_j are used.

3

Contributions

To use the theory mentioned before, it has to be implemented and evaluated. By doing so we came across several issues and new ideas to improve the existing algorithms. In this section the implementations and possible improvements are discussed. In the next section all these modifications will be evaluated on their performance. First the improvements to IKRA is discussed. Second Arnoldi and two-sided Arnoldi is improved and as third the participation factor is revisited.

3.1. Improvements to IRKA

The basic IRKA algorithm shown in Algorithm 3 often breaks down for the LTI systems used in topology optimization. The modifications made to the algorithm are to deal with singular matrices and to improve the stability of the algorithm.

For many realistic problems the stiffness matrix is singular in the second-order linear system. When the second-order system is rewritten to a first-order system the matrix A is singular as well. This singular matrix will cause problems for IRKA. The strength of IRKA lies with finding the optimal shifts σ, which are the mirror images of the poles of the reduced system. For reduced system where V contains a eigenvector the corresponding pole is zero and IRKA will use a shift of zero. This is a problem since IRKA tries to calculate $(A-\sigma E)^{-1}b$ and $(A-\sigma E)^{-*}c$ which are now $A^{-1}b$ and $A^{-*}c$, but A is singular thus the inverse does not exist. Due to the methods in Matlab and its computational precision, these operations still give a result, although the accuracy is questionable. To solve this problem the first few vectors with an eigenvalue of zero will be calculated differently. Some MOR methods decomposes the system in its eigenvectors/eigenmodes and use these to create a reduced system. This idea can be applied here since we know the eigenmodes/rigid body modes with eigenvalue zero. The standard IRKA can then be resumed for the other eigenvalues.

The second modification was made to improve the stability of the algorithm. First the vectors for V and W where chosen such that $v_i = (A-\sigma_i E)^{-1}b$ and $w_i = (A-\sigma_i E)^{-T}c$. In some cases the reduced model created with this V and W is stable, but unfortunately this is not true in general. Therefore to improve the stability we choose to evaluate the orthogonalization of V and W as well as evaluate the biorthogonalization of V and W. These methods are shown in Algorithm 6 and Algorithm 7 respectively. These algorithms aim to improve the stability, but are more expensive computational and timewise.

3.2. Improvements to Two-sided Arnoldi

The implementation of two-sided Arnoldi has been done by implementing Arnoldi twice as is shown in Algorithm 2. The matrices V and W are orthogonalized, since this is done in Arnoldi. This means $V^*V = I$ and $W^*W = I$.

The two improvements made for two-sided Arnoldi are mass-orthogonalizing the matrices V and W and using a preconditioner for W.

First we analyse the effect of a different orthogonalization method. Let $E = Q^*Q$. The relation between V and the mass orthogonalized $\widetilde{V} = Q^{-1}V$. Same holds for $\widetilde{W}$. This relation can be derived

from

$$\widetilde{V}^* E \widetilde{V} = I$$
$$\widetilde{V}^* Q^* Q \widetilde{V} = I$$
$$\text{if } \widetilde{V} = Q^{-1} V$$
$$V^* Q^{-*} Q^* Q Q^{-1} V = I$$
$$V^* V = I$$

For standard orthogonalization the first-order linear equation can be approached with the reduced system as follows

$$E\dot{x} = Ax + b \tag{3.1}$$
$$\dot{x} = E^{-1}Ax + E^{-1}b \tag{3.2}$$
$$x \approx Vz \tag{3.3}$$
$$V\dot{z} \approx E^{-1}AVz + E^{-1}b \tag{3.4}$$
$$W^*V\dot{z} \approx W^*E^{-1}AVz + W^*E^{-1}b \tag{3.5}$$
$$\text{if } (W^*V)^{-1} \text{ exist then}$$
$$\dot{z} \approx (W^*V)^{-1}W^*E^{-1}AVz + (W^*V)^{-1}W^*E^{-1}b \tag{3.6}$$
$$V\dot{z} \approx V(W^*V)^{-1}W^*E^{-1}AVz + V(W^*V)^{-1}W^*E^{-1}b \tag{3.7}$$
$$\dot{x} \approx V(W^*V)^{-1}W^*E^{-1}Ax + V(W^*V)^{-1}W^*E^{-1}b \tag{3.8}$$
$$\dot{x} \approx V(W^*V)^{-1}W^*(E^{-1}Ax + E^{-1}b) \tag{3.9}$$
$$\dot{x} \approx V(W^*V)^{-1}W^*Q^{-1}Q^{-*}(Ax + b) \tag{3.10}$$

For mass-orthogonalization the first-order linear equation are

$$E\dot{x} = Ax + b \tag{3.11}$$
$$x \approx \widetilde{V}\tilde{z} \tag{3.12}$$
$$E\widetilde{V}\dot{\tilde{z}} \approx A\widetilde{V}\tilde{z} + b \tag{3.13}$$
$$\widetilde{W}^*E\widetilde{V}\dot{\tilde{z}} \approx \widetilde{W}^*A\widetilde{V}\tilde{z} + \widetilde{W}^*b \tag{3.14}$$
$$W^*Q^{-*}EQ^{-1}V\dot{\tilde{z}} \approx W^*Q^{-*}A\widetilde{V}\tilde{z}W^TQ^{-*}b \tag{3.15}$$
$$W^*V\dot{\tilde{z}} \approx W^*Q^{-*}A\widetilde{V}\tilde{z} + W^*Q^{-*}b \tag{3.16}$$
$$\text{if } (W^*V)^{-1} \text{ exist}$$
$$\dot{\tilde{z}} \approx (W^*V)^{-1}W^TQ^{-*}A\widetilde{V}\tilde{z} + (W^*V)^{-1}W^*Q^{-*}b \tag{3.17}$$
$$\widetilde{V}\dot{\tilde{z}} \approx \widetilde{V}(W^*V)^{-1}W^*Q^{-*}A\widetilde{V}\tilde{z} + \widetilde{V}(W^*V)^{-1}W^*Q^{-*}b \tag{3.18}$$
$$\dot{x} \approx Q^{-1}V(W^*V)^{-1}W^*Q^{-*}Ax + Q^{-1}V(W^*V)^{-1}W^*Q^{-*}b \tag{3.19}$$
$$\dot{x} \approx Q^{-1}V(W^*V)^{-1}W^*Q^{-*}(Ax + b) \tag{3.20}$$

The two model approximation are

$$\dot{x} \approx V(W^*V)^{-1}W^*Q^{-1}Q^{-*}(Ax + b) \tag{3.21}$$
$$\dot{x} \approx Q^{-1}V(W^TV)^{-1}W^*Q^{-*}(Ax + b) \tag{3.22}$$

The two orthogonalization methods are the same when Q^{-1} commutes with $V(W^*V)^{-1}W^*$. For example when Q^{-1} is the identity matrix. The accuracy of the model is determined by how well the matrix $V(W^*V)^{-1}W^*$ approximates the identity matrix.

The second improvement for two-sided Arnoldi is to use the preconditioner $(A - \sigma E)^{-1}$ with the matrix W^* [11]. This new matrix $(A - \sigma E)^{-1}W^*$ can be calculated explicitly with $(A - \sigma E)^{-*}$ and W or it can be calculated implicitly by using a different Krylov space when creating W. First W was created with the Krylov space

$$\mathcal{K}_r(E^*(A - \sigma E)^{-*}, c). \tag{3.23}$$

This subspace is defined by

$$\text{span}\{c, E^*(A-\sigma E)^{-*}c, E^*(A-\sigma E)^{-*}E^*(A-\sigma E)^{-*}c, ...\}. \tag{3.24}$$

Multiplying each vector of W with the preconditioner is the same as multiplying W with the preconditioner. Thus the range of W should be

$$\text{span}\{(A-\sigma E)^{-*}c, (A-\sigma E)^{-*}E^*(A-\sigma E)^{-*}c, \tag{3.25}$$
$$(A-\sigma E)^{-*}E^*(A-\sigma E)^{-*}E^*(A-\sigma E)^{-*}c, ...\} \tag{3.26}$$

This can be described with the Krylov space $\mathcal{K}_r((A-\sigma E)^{-*}E^*, (A-\sigma E)^*c)$. This Krylov space will be evaluated with the use of the error plot for the test problems and with the condition number of the reduced matrix E_r. This condition number describes how sensitive a system is to small pertubations.

3.3. Improvements to Participation Factor

The participation factor proposed by Gu et al. explained in Section 2.4 was

$$p_i = \frac{|v_i^T s|}{[(v_i^T v_i)(s^T s)]^{1/2}} \tag{3.27}$$
$$s = (K + \Omega i D - \Omega^2 M)^{-1} b \tag{3.28}$$

with $v_i \in V$ and Ω a frequency of interest. This participation factor is equivalent to

$$p_i = \frac{|v_i^T s|}{[(v_i^T v_i)(s^T s)]^{1/2}} \tag{3.29}$$
$$s = (\Omega i E - A)^{-1} b \tag{3.30}$$

for first-order linear system. Two modifications are made to the participation factor to improve its results.

First modification is to include the mass matrix for the dot-products. This is chosen for two reasons. First, the basis vectors are mass-orthogonalized. Second, we want to prioritize the modes or points with a large mass since resonance of structures with a large mass have a bigger influence on the behaviour of the structure then the resonance of the structures with a smaller mass. This participation factor is described by

$$p_i = \frac{|v_i^T E s|}{[(v_i^T E v_i)(s^T E s)]^{1/2}} \tag{3.31}$$
$$s = (\Omega i E - A)^{-1} b \tag{3.32}$$

The second modification focuses on the influence of a basis vector in the output vector y instead of the state-variable x. To this end we define a new participation factor as

$$k_i = \frac{|v_i^T E s|}{\sqrt{(v_i^T E v_i)(s^T E s)}} \tag{3.33}$$
$$s = (\Omega i E - A)^{-1} b \tag{3.34}$$
$$p_i = k_i \frac{|c^T v_i|}{\sqrt{(v_i^T v_i)(c^T c)}} \tag{3.35}$$

The efficiency of these participation factors will be tested in combination with Arnoldi. To differentiate between the three participation factors, they will be called Gu's, Gu's with mass norm and the new/transferred participation factor.

4

Evaluation

To evaluate the algorithms and their modifications they will be examined using two examples. First, these examples will be introduced. Second, the location of the shift for shift-and-invert Arnoldi is discussed. Third, the reduced models of Arnoldi and shift-and-invert Arnoldi are compared. Fourth, the modification to the orthogonalization of shift-and-invert Arnoldi is shown. Fifth, the participation factors are discussed for shift-and-invert Arnoldi with the orthogonalization methods. Then the performance of IRKA and its modifications are discussed and lastly, the performance of shift-and-invert Arnoldi and IRKA are compared.

4.1. An Acoustic Example and a Topology Optimization Example

In this subsection two test examples are introduced to evaluate all the modifications made to the reduction methods. First, an acoustic example is described and second, a topology optimization example is introduced. Then the method to asses the accuracy of the reduced models is explained.

4.1.1. Acoustic Example

The fist example used to evaluate all the modifications of the MOR methods is an acoustic example discussed in [23]. This example models the propagation of sound in a room in two dimensions. One of the four walls is coated in sound-dampening material and has an absorbing boundary. The other walls have a reflective boundary.

The propagation of sound can be described by the wave equation

$$\frac{1}{c^2}\frac{\partial^2 p}{\partial t^2} = \triangle p \qquad \text{in } \Omega \tag{4.1}$$

with $\triangle$ the Laplace operator and with $c = 340$ m/s the speed of sound.

The reflective boundary is described by the homogeneous Neumann condition

$$\frac{\partial p}{\partial n} = 0$$

and the absorbing boundary is described by

$$\frac{\partial p}{\partial n} = -\frac{1}{cZ_n}\frac{\partial p}{\partial t}$$

with $Z_n = 0.2 - 1.5i$ the acoustic impendance of the wall.

This problem can be solved numerically with the FE method using triangular elements. Following all of the steps of FEM ,as shown in [23], the discretized quadratic eigenproblem is described by

$$\lambda^2 Mp + \lambda Cp + Kp = 0 \tag{4.2}$$

with M, C and K are the mass, dampening and stiffness matrices.

In the middle of the room is a sound source that excites the dynamical system and a sensor that records the sound. The dynamical system of this structure is described by

$$\begin{aligned} M\ddot{p} + C\dot{p} + Kp &= b \\ y &= c^T p \end{aligned} \tag{4.3}$$

The size of the matrices are 121 by 121. When this system is written to the first-order matrix equation the size of the matrices are 242 by 242.

4.1.2. Topology Optimization Example

The second problem used for the evaluations is taken from a two dimensional topology optimization. The design and evolution of the topology are shown in Figure 4.2 with iteration 0, 30 and 60. The two block at the bottom of the figure can be exited and the vibrations of the system are measured at the top of the structure.

The optimization process has the objective to maximize the smallest three eigenfrequencies. The objective and objective function are

$$\max_{\rho} \quad g_\Omega(\rho) \tag{4.4}$$

$$g_\Omega(\rho) = \sum_{i=1}^{3} \frac{1}{\Omega_i(\rho)} \tag{4.5}$$

with Ω_i is the i-th eigenfrequency of the dynamical system. The dynamical system is described by

$$\begin{aligned} M(\rho)\ddot{x} + K(\rho)x &= b \\ y &= c^T x \end{aligned} \tag{4.6}$$

The matrices, vectors and rigid body modes are provided by Arnoud Delissen, who did the optimization of this design. To evaluate the MOR methods we choose to use the matrices of the last iteration. The size of the matrices are 18914 by 18914. Since we rewrite it to a first-order linear system the matrices used for MOR are 37828 by 37828.

With the optimization of this topology only the location of the eigenfrequencies in the frequency band where considered in the objective. If it were possible to 'cheaply' calculate the frequency response function (FRF), then the area under the FRF or the height of the peaks could be included in the objective for the optimization. This is where model order reduction methods could be used to improve topology optimization.

4.1.3. How to Asses the Accuracy

To determine the accuracy of the model order reduction methods and their modifications we check how well the FRF of the reduced models matches the FRF of the full model. This is done with the help of two Matlab functions. *sparss* to create sparse first-order state-space model object and *sigma* for the frequency response of the model. The response in the frequency response function is the imaginary part of $H(\omega i)$, with ω the frequency. It is scaled to decibel by

$$dB(x) = 20\log_{10}(x). \tag{4.7}$$

The accuracy is assessed both visually and numerically. Visually by checking how well the first few peaks of the reduced system match and how big the reduced system should be to match the full system. Numerically by calculating the difference in the response between the full system and the reduced system at the different frequency points.

4.2. Preconditioner used for Two-Sided Arnoldi

The preconditioner used for two-sided Arnoldi is $(A - \sigma E)^{-1}$. In both examples the preconditioner increases the accuracy of the reduced model significantly. Figure 4.3 shows the increased accuracy for the acoustic example. This is done by plotting the error of the reduced models with and without the

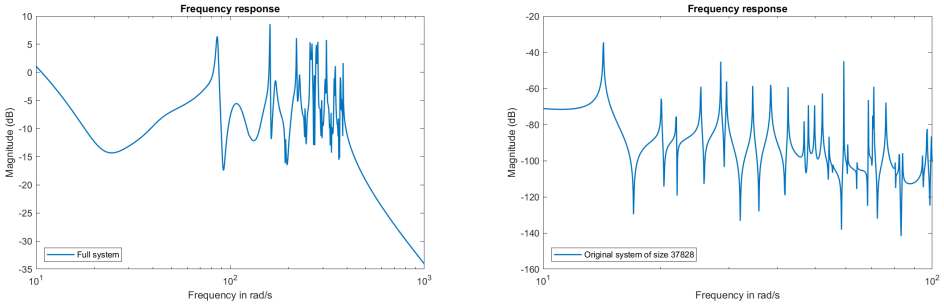

(a) the FRF for the room

(b) The FRF of the structure in topology optimization

Figure 4.1: The frequency response function for the two examples

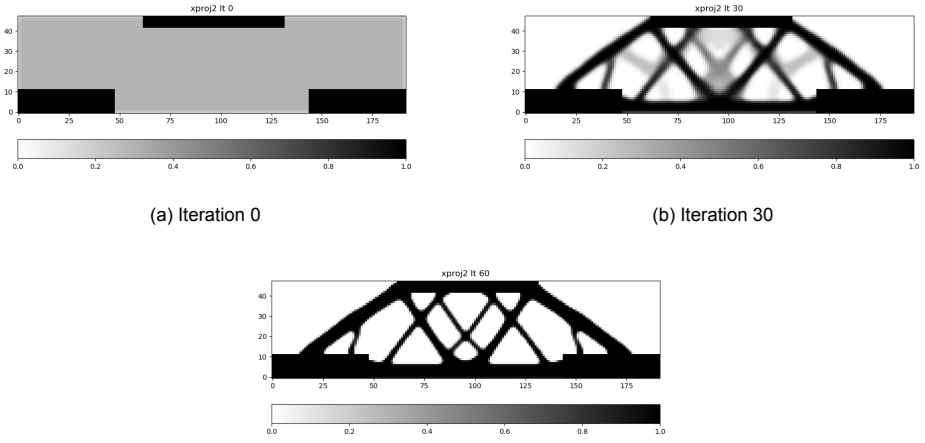

(a) Iteration 0

(b) Iteration 30

(c) Iteration 60

Figure 4.2: Evolution of the topology

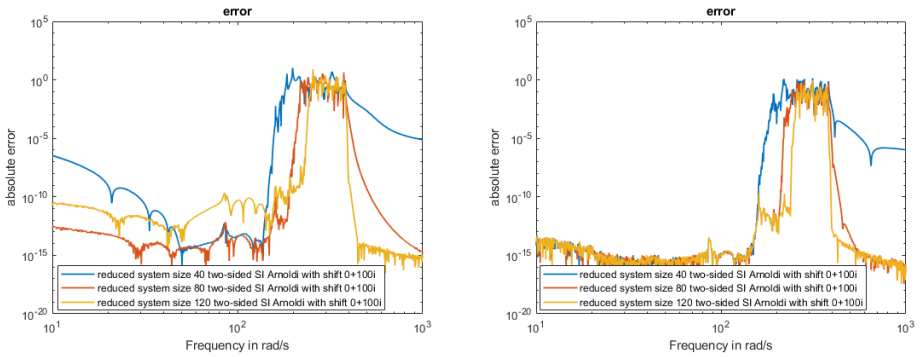

(a) Without Preconditioner (b) With Preconditioner

Figure 4.3: The error of the reduced model of size 40, 80 and 120 with and without the use of a preconditioner for the acoustic example

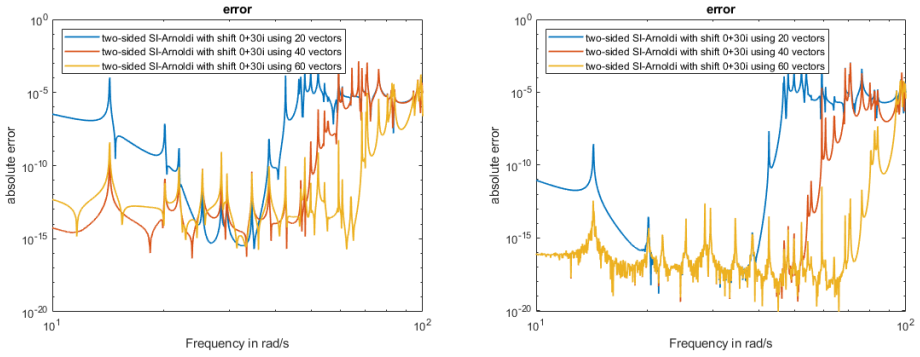

(a) Without Preconditioner (b) With Preconditioner

Figure 4.4: The error of the reduced model of size 20, 40 and 60 with and without the use of a preconditioner for the topology example

use of a preconditioner. The figure on the left side shows the error for the reduced models of size 40, 80 and 120 without the preconditioner and on the right side the error is shown for the same models with the use of a preconditioner. The figure shows clearly that the use of a preconditioner decreases the error significant.

An error plot for topology optimization example is also made and is shown in Figure 4.4. Here the reduced models are of size 20, 40 and 60. This figure shows as well that the error decreases when a preconditioner is used.

The increasing accuracy might be explained with the condition number of E_r, since for the reduced model the equation $E_r\dot{x}_r = A_r x_r + b_r$ or $\dot{x}_r = E_r^{-1}A_r x_r + E_r^{-1}b_r$ is used. For different sizes of the reduced model the condition number is shown in Table 4.1 for both examples.

For the acoustic example the condition number does not change for E_r when a preconditioner is used with W. For the example of topology optimization the condition number does change with a factor 100. Although this condition number does not fully covers the reason to why the preconditioner improved the system, the preconditioner will be used further on as it showed an improved accuracy in the error plot.

4.3. The Location of the Shift for the Shift-and-Invert Arnoldi's

The location of the shift determines how well the reduced model performs. For these locations there are various options to choose from. The shift can be real and larger than the absolute largest eigenvalues [20] or the shift can be strictly imaginary and in the interested frequency domain. This gives a better approximation locally, but has slow convergence globally [11]. A third option is combining these shifts to get a complex shift [8]. Since we are only interested in matching the peaks around the smallest eigenfrequencies the imaginary shifts are probably best to use, but for completeness we will evaluate

size of model	Acoustic		Topology optimization	
	W	$(A-\sigma E)^{-1}W$	W	$(A-\sigma E)^{-1}W$
5	X	X	121	41
6	7.8	4.05	150	12
10	12	14	1.9e4	13
20	2e4	1.5e4	8.7e4	8.9e3
30	3e4	1.25e5	3.9e7	1e4
40	5e4	1.7e5	3.9e6	4.8e4
50	4.6e4	1.35e5	7.6e7	1e5
60	1.3e5	5.9e5	1.2e8	3.3e6
70	2.6e5	4e5	2.5e9	1.4e6
80	2.6e5	3.5e5	1.5e8	6.7e6
90	1.6e5	3.2e5	6.3e9	3.6e7
100	2.6e5	5.6e5	5.5e8	2.9e8

Table 4.1: Condition number of the matrix E_r for different sizes of a reduced model created with two-sided Arnoldi with and without the preconditioner

a real shift and a complex shift as well. The five options discussed for the shift are

- imaginary shift at the start of the frequency domain
- imaginary shift in the middle of the frequency domain
- imaginary shift at the end of the frequency domain
- real shift larger than the eigenfrequencies in the frequency domain
- complex shift with an imaginary part in the middle of the domain and real part larger than the largest eigenfrequency

The best performing shift will be used in the other evaluations.

4.3.1. Acoustic Example

The frequencies of interest for the acoustic example are between 10 and 1000 rad/s. Therefore the imaginary shifts are chosen as $10i$, $100i$ and $1000i$. The real shift should be larger than the eigenfrequencies in the frequency domain. In Figure 4.1a it shows that the largest eigenfrequency lies around 400 rad/s. A safe choice for this shift would be 500. The complex shift should be a combination between the real shift and an imaginary shift in the middle of the domain, thus the complex shift used is $500 + 100i$.

For the evaluation of the imaginary shifts we used a reduced model of size 70. The frequency response functions of the different shifts are shown in Figure 4.5. The blue line in these figures is the response function of the full system and should be matched by the red line, which is the frequency response of the reduced system. One of the criteria to judge the reduced model was how well the reduced system matches the first few peaks of the full system. At first glance we can see that a shift of $1000i$ does not satisfy this criteria. To judge the accuracy we also plotted the error of the three methods as is shown in Figure 4.6. For both the shifts $10i$ and $100i$ the accuracy at the start is close to machine precision (approximately 10^{-16}) and a shift of $100i$ holds this accuracy for a larger bandwidth, therefore we can conclude this shifts performs the best of the three imaginary shifts.

For the evaluation of the real shift 500 we tested different sizes of the reduced model. The frequency responses are shown in Figure 4.7a. To match the first few peaks the reduced model has to be of size 100. To visually match the frequency response of shift $100i$ the reduced model with a real shift is of size 140. In Figure 4.7b we have plotted the error of the response of the various reduced model. When the reduced model with real shift of size 70 is compared with the imaginary shift $100i$ the error is worse with a factor of 10^9. For the larger models the accuracy goes to 10^{-12}, which is still worse than when an imaginary shift was used.

For the evaluation of the complex shift $500 + 100i$ the reduced models are of size 70, 100, 120 and 140. This is chosen to make the results of the response function comparable with the results of

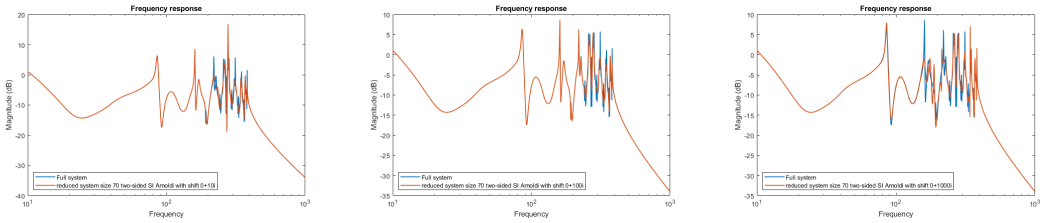

(a) Shift of $10i$ (b) Shift of $100i$ (c) Shift of $1000i$

Figure 4.5: Acoustic example with imaginary shifts

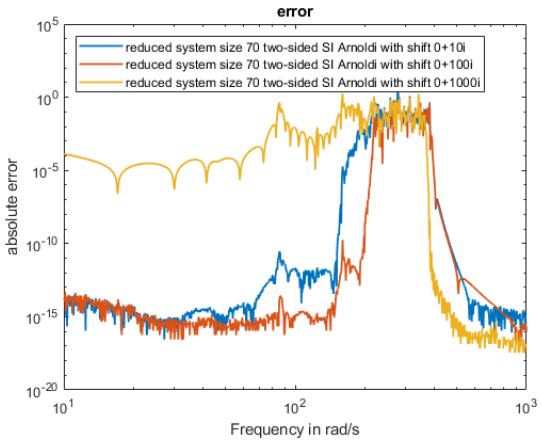

Figure 4.6: Error plot of the reduced systems with imaginary shift for the acoustic example

the response function of the reduced model using a real shift. In Figure 4.8 the performance of the reduced models and the error are shown. For the use of a complex shift and a real shift both the response function behaves similar and both errors are of the same magnitude. Since both perform worse than the imaginary shift we will use a shift of $100i$ in further evaluations.

4.3.2. Topology Optimization Example

In the topology optimization example we try to match the frequencies between 10 and 100 rad/s. The pure imaginary shifts tested are $10i$, $30i$ and $100i$. For the real shifts multiple values are tested, but since they all perform similar we will discuss only the shift 250. The complex shift is a combination of the real and imaginary shift and is thus chosen as $250 + 30i$.

For the imaginary shifts $10i$, $30i$ and $100i$ a reduced model of size 50 is used to evaluate the response function. The FRF of these shifts is shown in Figure 4.9. The blue line is the frequency response of the full system and the response of the reduced models is shown in red. In this figure we can see that a shift at $100i$ matches the response at higher frequencies, but not at the lower frequencies. Both the shifts $10i$ and $30i$ can match the response at the lower frequencies well, but struggle at the higher frequencies. Since we focus on matching the lower frequencies a shift of $100i$ is not preferred. Visually the best shift to use is $30i$. This is further confirmed by the error plot of the three shifts shown in Figure 4.10.

For the evaluation of the real shift 250 we tested different sizes of the reduced system as is shown in Figure 4.11a. The blue line is the response of the full system which should be matched by the reduced models. The frequency response function of the model of size 50 is terrible. This already demonstrates that a real shift performs worse than an imaginary shift. The reduced models starts to approximate the response of a few peaks at 150 vectors. We can see that this reduced model starts to find the location of the peaks, but not the height. When the reduced model is of size 200 it matches the response function of the full system. The error of these three different sizes of the reduced model are shown in Figure 4.11b. We see that the accuracy increases by increasing the size of the reduced model, but the error is still much worse than for the reduced model with an imaginary shift.

The complex shift used in this example is $250 + 30i$. The accuracy of the reduced models are

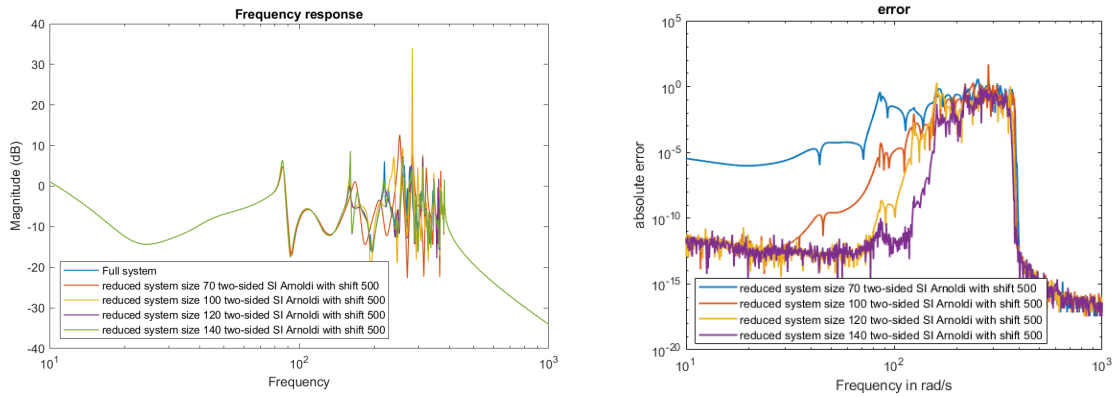

(a) Reduced model of size 100, 120 and 140

(b) Error of the reduced systems

Figure 4.7: Various reduced models with a real shift and its error for the acoustic example

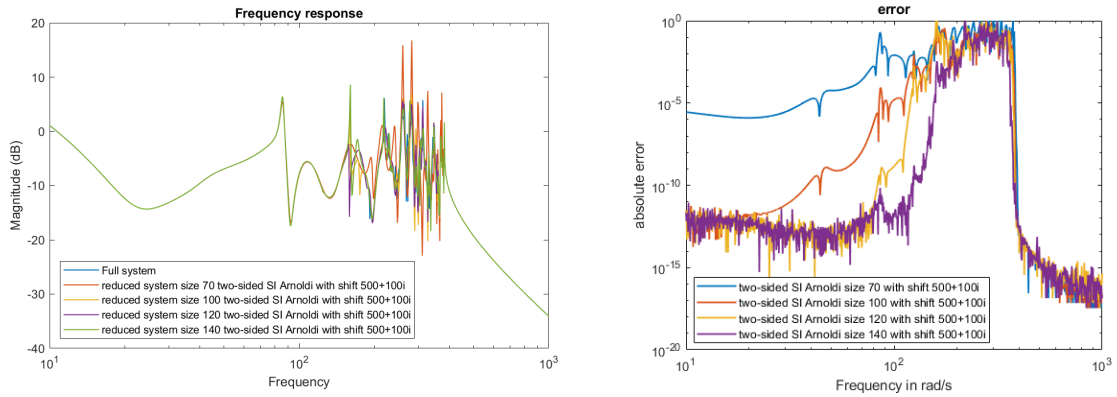

(a) Reduced model of size 100, 120 and 140

(b) Error of the reduced systems

Figure 4.8: Various reduced models with a complex shift and its error for the acoustic example

evaluated for the sizes 50, 150 and 200. The response function for these models are shown in Figure 4.12 together with the error. Again a reduced model of size 50 performs worse than when a imaginary shift is used. The FRF of these three models are similar to the FRF when a real shift is used. Still, the best shifts are the pure imaginary shifts. In further evaluations shift-and-invert Arnoldi will use $30i$ as a shift for the example of topology optimization.

4.4. Arnoldi vs Two-Sided Arnoldi

For MOR a commonly used method is Arnoldi. Previously we discussed that Arnoldi matches r moments of the transfer function for a reduced system of size r. We also mentioned that two-sided Arnoldi could improve the reduced system for it matches $2r$ moments. In this section we evaluate the perfor-

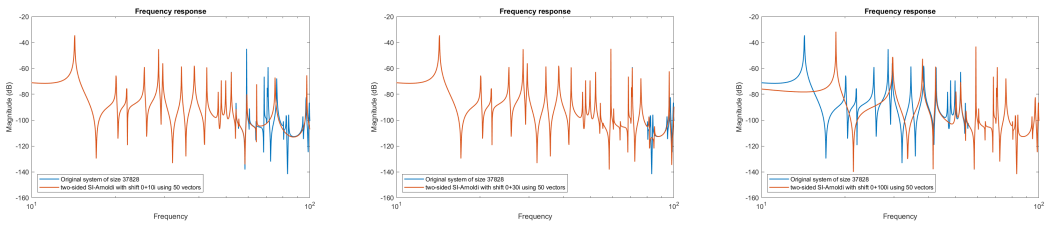

(a) Shift of $10i$

(b) Shift of $30i$

(c) Shift of $100i$

Figure 4.9: Reduced models of size 50 using imaginary shift for the topology optimization example

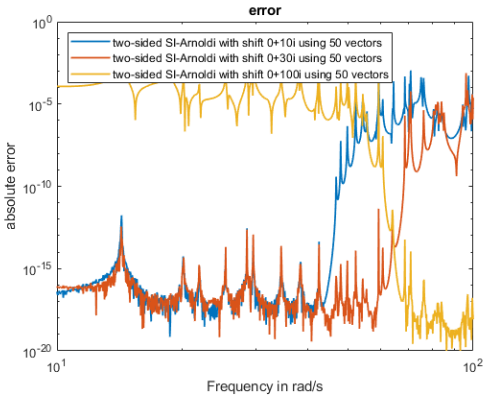

Figure 4.10: Corresponding error of the reduced models in Figure 4.9 for the topology optimization example

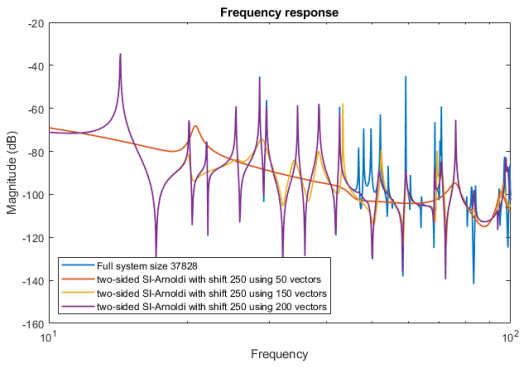

(a) Reduced model of size 50, 150 and 200

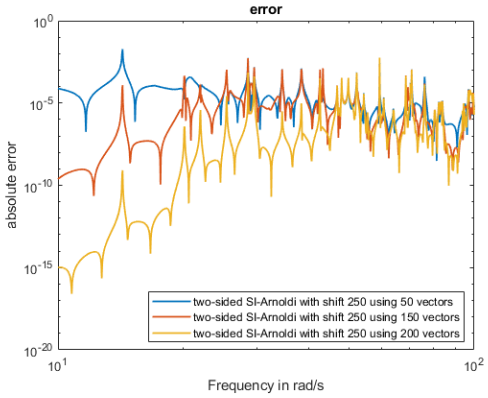

(b) Error of the reduced systems

Figure 4.11: Various reductions with a real shift and its error for topology optimization example

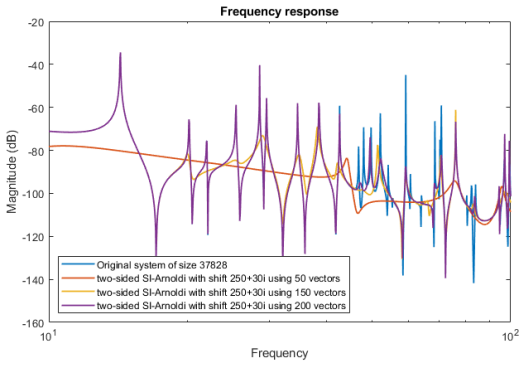

(a) Reduced model of size 50, 150 and 200

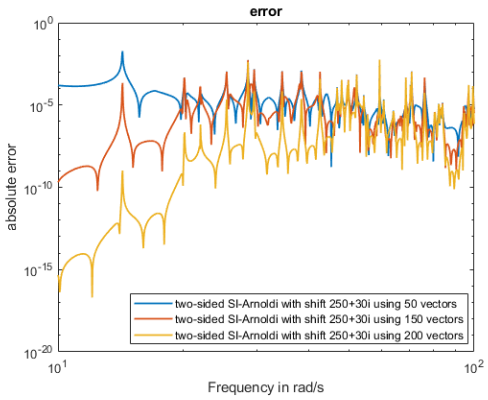

(b) Error of the reduced systems

Figure 4.12: Various reductions with a complex shift and its error for the topology optimization example

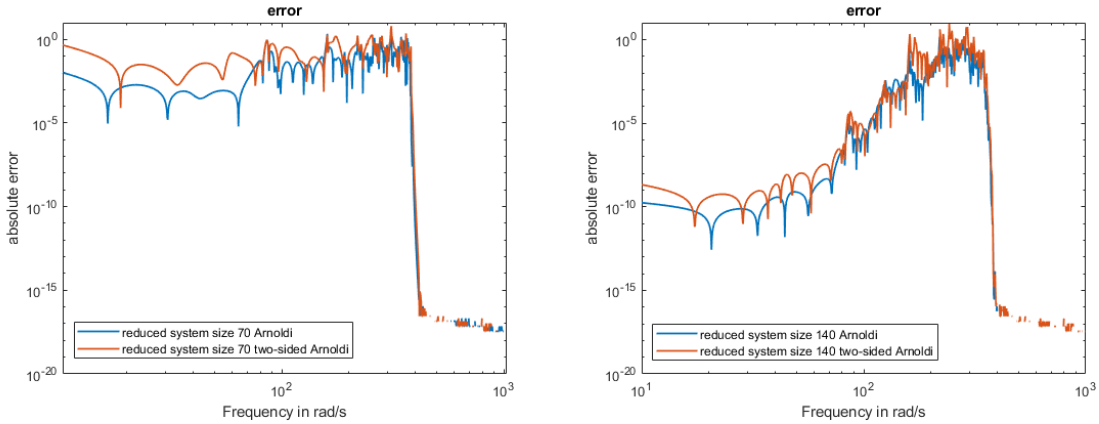

(a) Error of the different Arnoldi's for a model of size 70

(b) Error of the different Arnoldi's for a model of size 140

Figure 4.13: Arnoldi and two-sided Arnoldi for Acoustic Problem

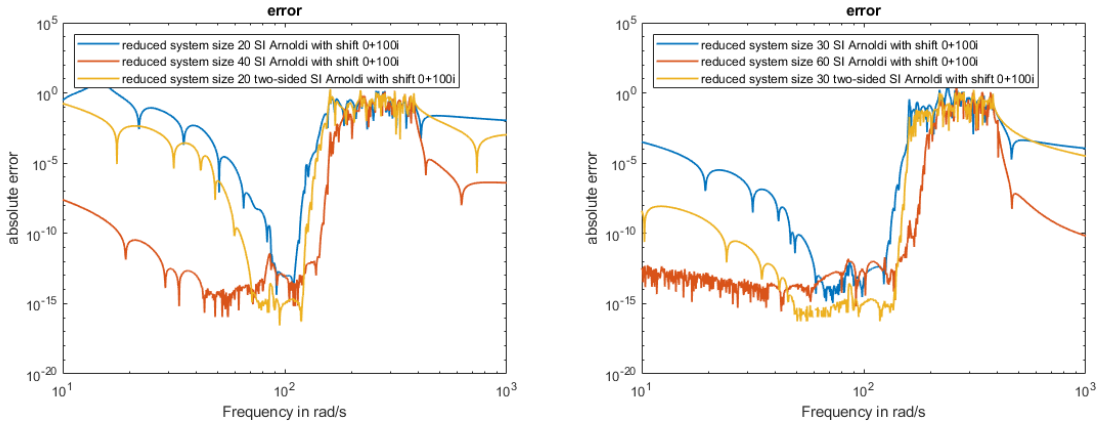

Figure 4.14: Error of the SI Arnoldi and two-sided SI Arnoldi for Acoustic Problem

mance of Arnoldi versus two-sided Arnoldi and the performance of shift-and-invert (SI) Arnoldi versus two-sided SI Arnoldi.

4.4.1. Acoustic Example

To evaluate the accuracy of the different method we will only look at the error of the reduced models. For the standard Arnoldi methods we tested a reduced model of size 70 and 140. The error is shown in Figure 4.13. For both sizes Arnoldi performs better than two-sided Arnoldi. This is not necessarily contradicting the theory discussed before, since these reduced models matches the transfer function around the point infinity. Thus two-sided Arnoldi should perform better at the higher frequencies. These frequencies lie outside the domain of interest.

The performance of the SI Arnoldi methods are evaluated by comparing the error of the model created by two-sided Arnoldi with the error of the model created by Arnoldi. First the comparison is done for the same size reduced models and second the comparison is done between a reduced model created with two-sided Arnoldi and a reduced model of twice the size created with standard Arnoldi. The second comparison is to evaluate the models when they match the same number of moments in the transfer function. Figure 4.14 shows two error plots. First one shows Arnoldi of size 20 and 40 and two-sided Arnoldi of size 20, the second error plot shows Arnoldi of size 30 and 60 and two-sided Arnoldi of size 30. Both figures show that the reduced model created with two-sided Arnoldi performs better than the reduced model of Arnoldi of the same size. When two-sided Arnoldi is compared with the larger Arnoldi model it shows that two-sided is locally more accurate than the larger Arnoldi model and when both increases two-sided Arnoldi gets more accurate over a bigger bandwidth than the larger Arnoldi model.

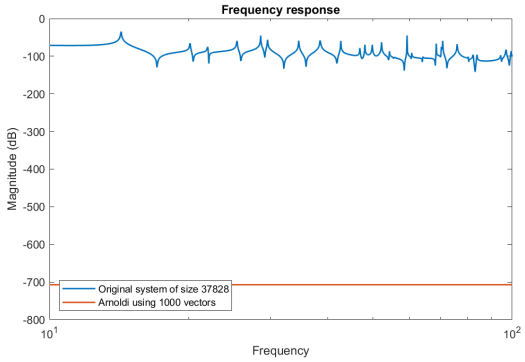

Figure 4.15: FRF of reduced model created with Arnoldi of size 1000 for topology optimization example

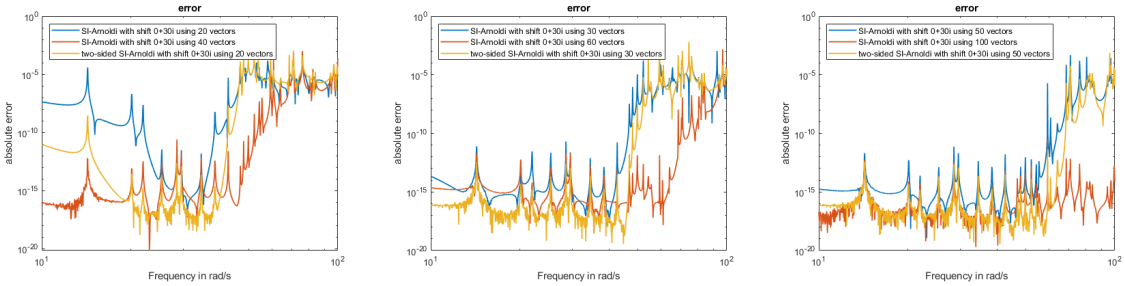

(a) Error of Arnoldi and two-sided Arnoldi with reduced size 20

(b) Error of Arnoldi and two-sided Arnoldi with reduced size 30

(c) Error of Arnoldi and two-sided Arnoldi with reduced size 50

Figure 4.16: Error of SI Arnoldi and two-sided SI Arnoldi with a shift of $30i$ for topology optimization

4.4.2. Topology Optimization Example

For the topology optimization example only the shift-and-invert Arnoldi methods are tested, because the reduced models created with the standard Arnoldi methods needs to be enormous before it starts to approximate the FRF. An example is shown in Figure 4.15 where a reduced model of size 1000 is used, created with Arnoldi.

Shift-and-invert Arnoldi methods will be evaluated similar to the acoustic example. Comparing the error of a model using two-sided Arnoldi with a model using Arnoldi of the same size and of twice the size of the model created with two-sided Arnoldi. In Figure 4.16 the error of the models are shown with two-sided Arnoldi of size 20, 30 and 50. In every figure we see that two-sided Arnoldi (yellow line) performs better than Arnoldi of the same size (blue line). For the big model of Arnoldi the figure shows that two-sided Arnoldi is more accurate near the location of the shift, but is less precise further away from the shift. When the model created with two-sided Arnoldi increases is size, the model becomes more accurate on a larger frequency domain than a model created with Arnoldi of twice it size.

4.5. Orthogonalization Methods for Two-Sided Shift-and-Invert Arnoldi

For two-sided Arnoldi different orthogonalization methods are evaluated. These are the standard method (orthogonalizing V and W such that $V^*V = I$ and $W^*W = I$) and mass-orthogonalization ($V^*EV = I$ and $W^*EW = I$). In theory the choice of orthogonalization methods should not affect the result of the model order reduction.

4.5.1. Acoustic Example

To evaluate the difference between standard orthogonalization and mass-orthogonalization the error of the reduced models are compared for the sizes 20, 30 and 40. This is shown in Figure 4.17. When the error is not close to machine precision the error for both orthogonalization methods are identical.

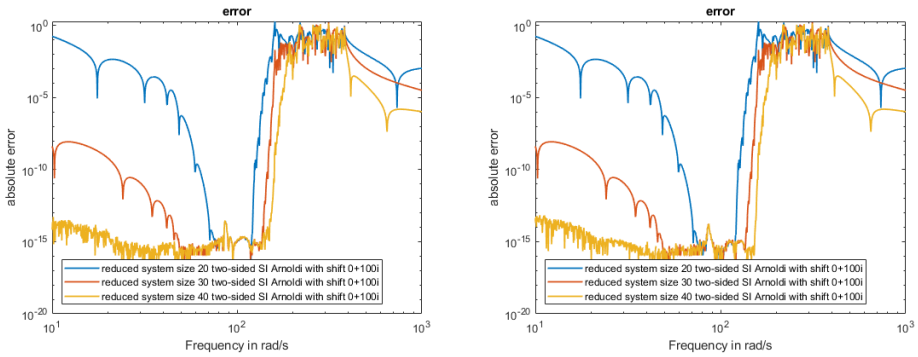

(a) standard orthogonalization (b) mass-orthogonalization

Figure 4.17: Reduced models with different orthogonalization methods for the acoustic example

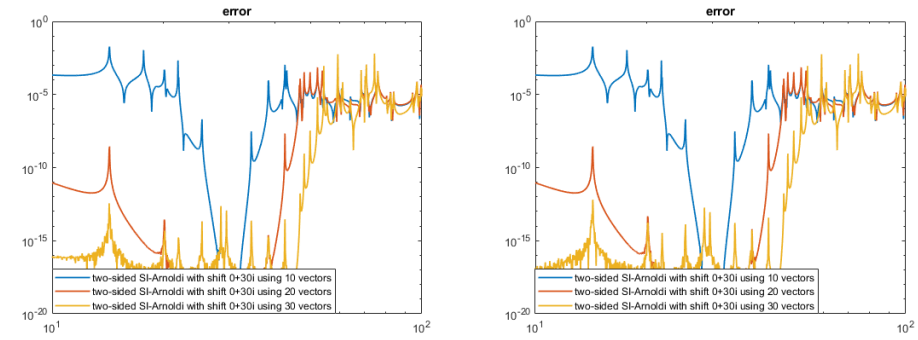

(a) Standard orthogonalization (b) mass-orthogonalization

Figure 4.18: Reduced models of size 10, 20 and 30 with different orthogonalization methods for the topology example

4.5.2. Topology Optimization Example

The difference in the orthogonalization methods are evaluated by comparing the error of the reduced models. The error of the reduced models of size 10, 20 and 30 are shown in Figure 4.18. Again the error of the reduced models of the same size are identical for standard orthogonalization and mass-orthogonalization.

4.6. The Three different Participation Factors

In this section three different participation factors are discussed to help reduce the size of the reduced models even further. They are used for the models created with two-sided Arnoldi in combination with standard orthogonalization and mass-orthogonalization. The three participation factors are called Gu's, Gu's with mass and the transferred participation factor.

4.6.1. Acoustic Example

In this example we start with a reduced model of size 100. Although it is shown before that the reduced model is already accurate for a smaller models a large model is chosen to show the effects of the participation factor.

For the use of the participation factors a few variables have to be determined beforehand. These are the frequency or frequencies of interest and the tolerance of the participation factor. Since we are interested in matching the first few peaks of the response function we choose Ω as

$$[10 \quad 90 \quad 200]$$

To determine the tolerance for each of the different participation factor method the values are calculated as mentioned in Section 3.3, Since the choice of orthogonalization influences the participation factor we plot them in two different figures. In Figure 4.19 are the three different participation methods shown

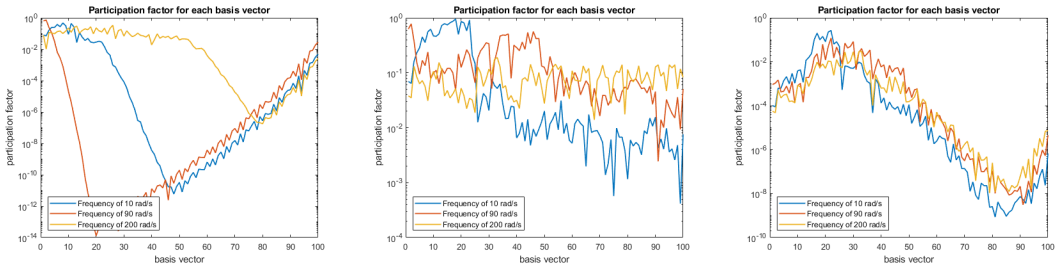

(a) Gu's (b) Gu's with mass (c) Transferred

Figure 4.19: The three different participation factors with orthogonalized V and W for the acoustic example

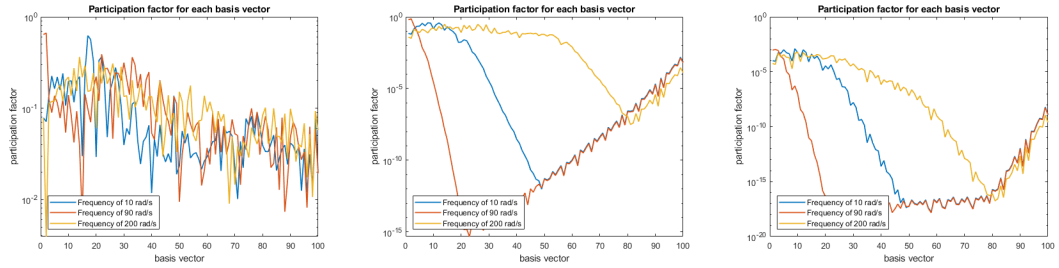

(a) Gu's (b) Gu's with mass (c) Transferred

Figure 4.20: The three different participation factors with mass-orthogonalized V and W for the acoustic example

for the orthogonalized V and W and in Figure 4.20 this is done with the mass-orthogonalization. Each line corresponds to a different value of Ω.

In three of the six graphs it clearly shows how large the reduced model should be to included certain frequencies in its approximation. These figures are the participation factor with Gu and standard orthogonalization and the participation factors Gu with mass and the new one with mass-orthogonalization of the vectors. It is clear to see that frequency 90 can be captured with less than 20 vectors and the frequency 200 around 60 to 80 vectors. One strange behaviour of these graphs are the increasing values after the sharp decline. For the other three graphs the importance of the vectors for the different frequencies are unclear.

To show the effects of a given tolerance the error of the frequency response function of the reduced models are calculated with multiple tolerances. This is shown in Figure 4.21. For Gu and Gu with mass the tolerance chosen is

$$[10^{-2} \quad 10^{-3} \quad 10^{-4} \quad 10^{-5}]$$

The reduced model decreases to a size between 59 and 87. For the transferred participation factor the tolerance is chosen as

$$[10^{-6} \quad 10^{-7} \quad 10^{-8} \quad 10^{-9} \quad 10^{-10}]$$

The reduced model decreases to a size between 43 and 67. To summarize the inclusion of a participation factor helps to reduce the size of the reduced model even further. One downside to the use of the participation factor is you have to guess the tolerance in advance.

4.6.2. Topology Optimization Example

Again we start with a large reduced model to show the effects of the participation factor. In this example the reduced model to start with is of size 100 The Ω's in this example are chosen as

$$[10 \quad 25 \quad 50 \quad 80].$$

As mentioned before the orthogonalization of the vectors in V and W influences the behavior of the participation factors. In Figure 4.22 the vectors are standard orthogonalized for the three methods and in Figure 4.23 the vectors are mass-orthogonalized. Each line corresponds to a different value of Ω.

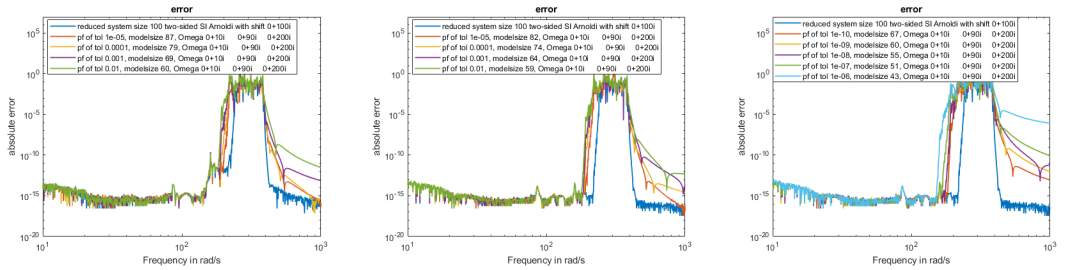

(a) Error of Gu's (b) Error of Gu with mass (c) Error of the new participation factor

Figure 4.21: Multiple tolerances used with the participation factors

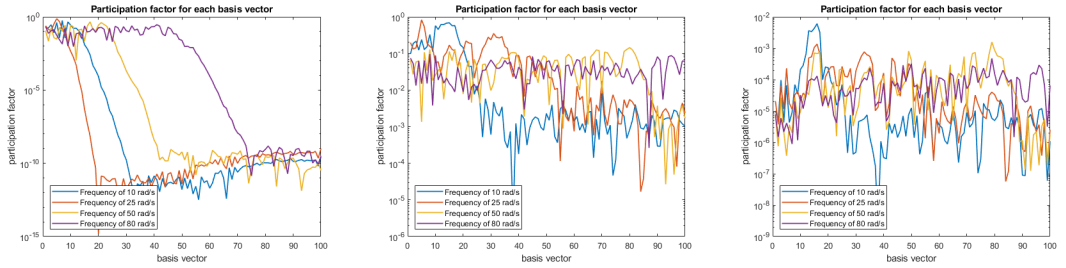

(a) Gu's (b) Gu's with mass (c) Transferred

Figure 4.22: The three different participation factors with orthogonalized V and W for the topology example

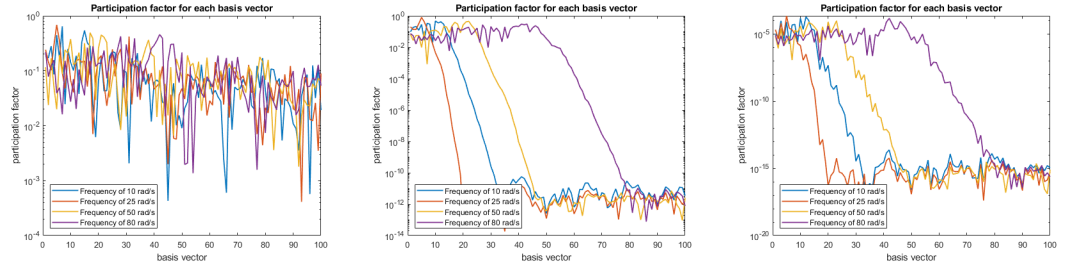

(a) Gu's (b) Gu's with mass (c) Transferred

Figure 4.23: The three different participation factors with mass-orthogonalized V and W for the topology example

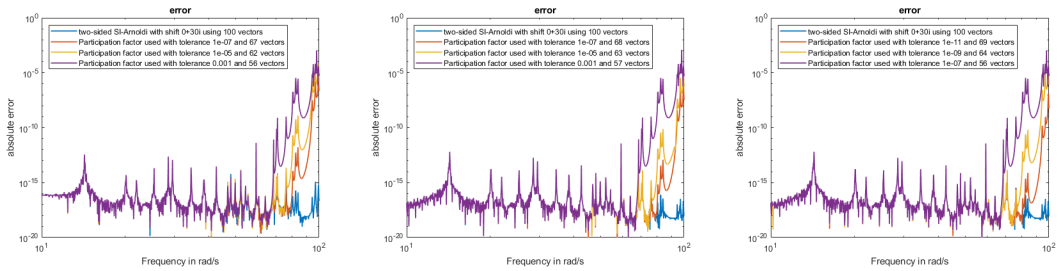

(a) Error of Gu's for tolerance 10^{-3}, 10^{-5} and 10^{-7}

(b) Error of Gu's with mass for tolerance 10^{-3}, 10^{-5} and 10^{-7}

(c) Error of the new participation factor for tolerance 10^{-7}, 10^{-9} and 10^{-11}

Figure 4.24: Multiple tolerances used with the participation factors

In these two figures there are three graphs that show a usable participation factor and it is clear to see that the participation factor should use a vector norm corresponding with the method of orthogonalization. For Gu's participation factor the MOR method should use standard orthogonalization for the basis and for Gu's with mass and the transferred participation factor this means using model order reduction with mass-orthogonalization.

The three graphs of the participation factors indicates how large the reduced model should be to capture certain frequencies. They all show that with a reduced model of size 20 the frequency 25 is captured and with a reduced model of size 50 they capture the frequencies 10, 25 and 50.

Normally a tolerance should be guessed in advance, but here we only evaluate multiple tolerances for the different participation factors. The error of the response function is shown in Figure 4.24. For Gu and Gu with mass the tolerances used are

$$[10^{-3} \quad 10^{-5} \quad 10^{-7}]$$

and for the transferred participation factor the tolerance used is

$$[10^{-7} \quad 10^{-9} \quad 10^{-11}]$$

The reduced model decreases its size independent of which participation factor to be between 55 and 70.

4.7. IRKA with Orthogonalization Methods

For IRKA two modifications where suggest to improve the algorithm. These are including an orthogonalization method and including the rigid body modes (rbm). In this section the orthogonalization will be discussed.

4.7.1. Acoustic Example

IRKA without any modifications made to it performs terrible. The idea behind IRKA is finding iteratively the optimal shifts for the reduced model, but at the moment it can do only three iterations before the algorithm crashes. This crash starts when it calculates v_i and w_i with entries of infinity and then calculating the new shifts. The largest reduced model to create without crashing is of size 10. This model can only match the first peak and is shown in Figure 4.25.

IRKA improves significantly when one of the orthogonalization methods is included. The algorithm will now run until the shifts stop changing much between iterations or when the limit of iterations is reached. The response function of the reduced models with both orthogonalization methods is shown in Figure 4.26 for the sizes 20,60 and 100. The functions are not very precise, but it matches the location of all the peaks and valleys of the function. It became clear when evaluating the error plot that one orthogonalization method is not better than the other. It changes for different reduced model sizes as is shown in Figure 4.27 for the sizes 50,70 and 100. The difference might be caused by the location of the shifts, since the algorithm determines iteratively the location of its shifts and the optimal location does not have to be unique.

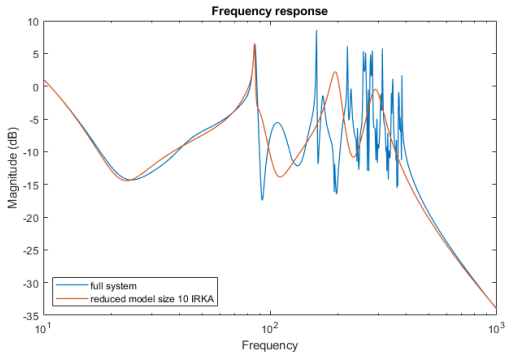

Figure 4.25: IRKA without modifications for the acoustic example

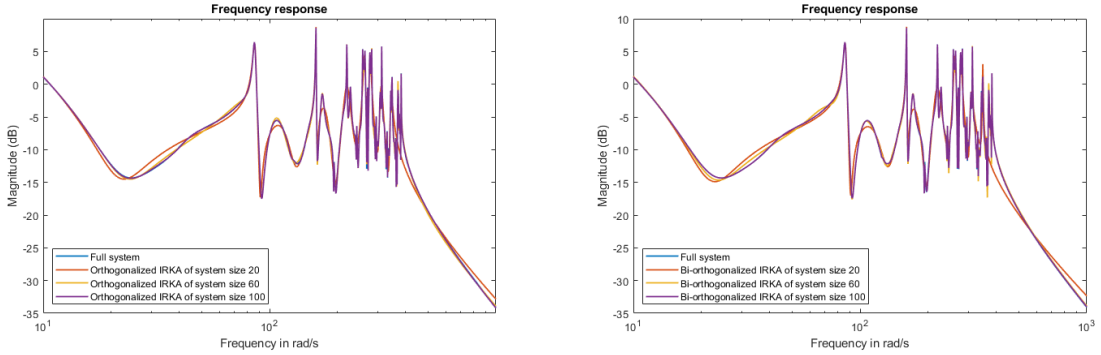

(a) Orthogonalization (b) Bi-orthogonalization

Figure 4.26: Orthogonalization and bi-orthogonalization used with IRKA for the acoustic example

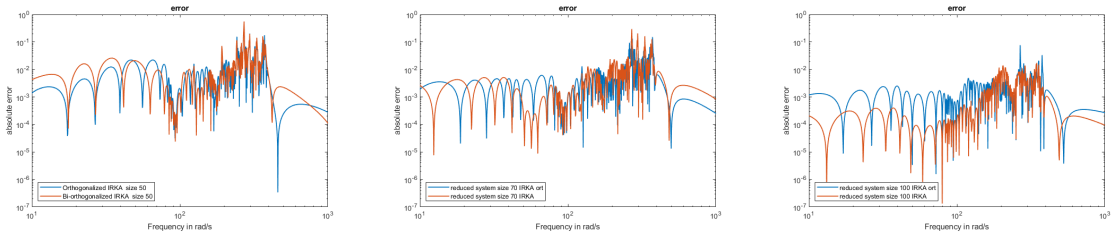

(a) Reduced model of size 50 (b) Reduced model of size 70 (c) Reduced model of size 100

Figure 4.27: Error of IRKA with orthogonalization and biorthogonalization methods for the acoustic example

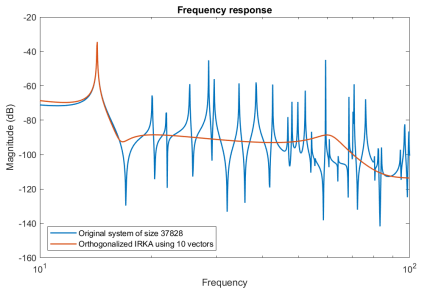

Figure 4.28: IRKA without modifications for topology optimization

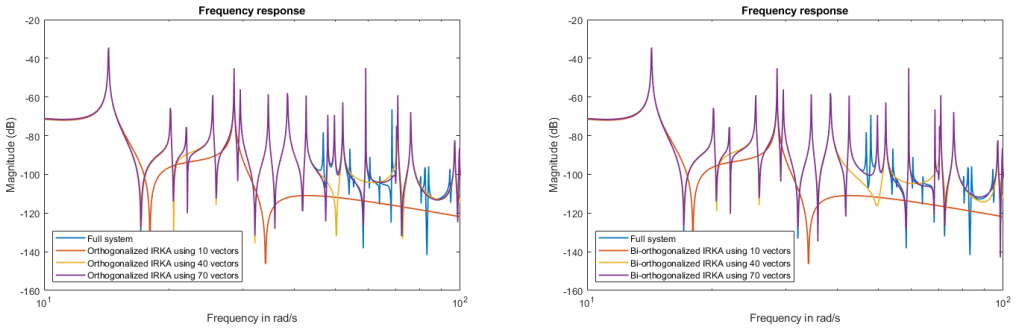

(a) Orthogonalization (b) Bi-orthogonalization

Figure 4.29: Orthogonalization and bi-orthogonalization used with IRKA for the topology optimization example

4.7.2. Topology Optimization Example

IRKA without any modifications crashes after four iterations due to numerical instability. This is caused by a singular matrix V and/or W, which means the vectors in that matrix are linear dependent. That, in turn, creates singular matrices A_r and E_r. The last stable iteration for a reduced model of size 10 has a frequency response function which only matches one peak, as is shown in Figure 4.28.

IRKA is improved significantly when either of the orthogonalization methods is included. For both methods IRKA does not crashes after four iterations and the reduced models can be increased in size. To show this the FRF is shown in Figure 4.29 for the reduced models of size 10, 40 and 70 with orthogonalization and with biorthogonalization of the vectors in V and W. At first glance the orthogonalization methods perform similar with only a small difference around frequency 50 rad/s.

To evaluate the accuracy we focused on the frequency between 10 and 50 rad/s. The error plot is shown in Figure 4.30. The two most noticable differences are first the accuracy for the reduced model of size 40 with biorthogonalization is higher at the lower frequency with a factor 10 and second, with orthogonalization the reduced models are more accurate around 35 rad/s. Overall one is not clearly better than the other.

4.8. IRKA with Rigid Body Modes

For IRKA two modifications where suggest to improve the algorithm. These are including an orthogonalization method and including the rigid body modes (rbm). In this section the rigid body modes will be discussed with and without the inclusion of the orthogonalized V and W.

4.8.1. Acoustic Example

First IRKA crashed after a few iterations for a very small model when no modifications where made to it. Now the performance of IRKA is improved when the rigid body modes are included in the algorithm. It can create a reduced model of size 14 without a limit on the number of iterations. This model is still far from a good approximation as can be seen in Figure 4.31. For larger models the algorithm still crashes as it did before.

When IRKA is combined with rigid body modes and one of the orthogonalization methods then the

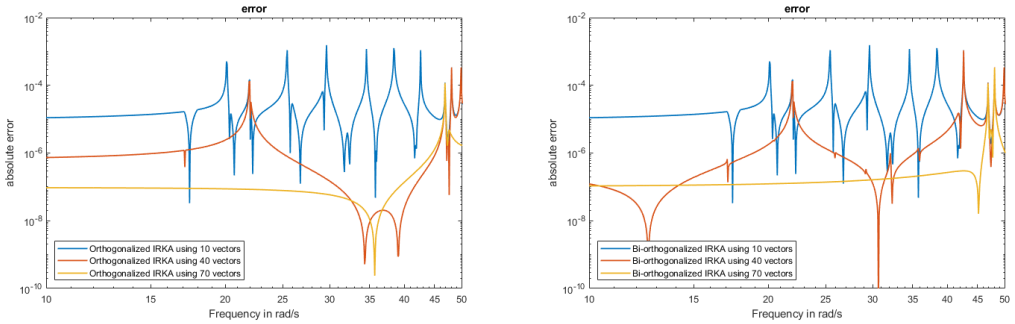

(a) Error for orthogonalization method

(b) Error for bi-orthogonalization method

Figure 4.30: Error of the reduced models of size 10, 40 and 70 with IRKA and the orthogonalization methods for the topology optimization example

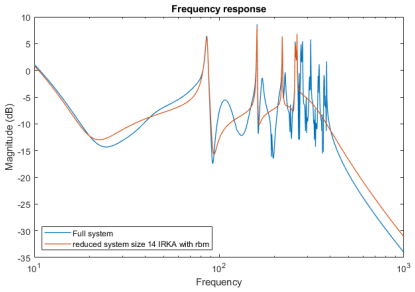

Figure 4.31: IRKA with rigid body modes for the acoustic example

accuracy increases and the reduced model can be much larger compared with IRKA using only the rigid body modes.

When IRKA with rigid body modes and orthogonalization is compared with IRKA using only orthogonalization it is as accurate or slightly less acurate. This is the case for both orthogonalization methods. In Figure 4.34 the error is shown for both methods using the regular orthogonalization method. The reduced models are of size 50, 70 and 100.

4.8.2. Topology Optimization Example

The inclusion of the rigid body modes also improves the results for the example of topology optimization. Without any modifications the largest model created with IRKA was of size 10. With the inclusion of the rigid body modes IRKA can reduce the system to a model of size 27. The response of this model is shown in Figure 4.33. For a larger model the algorithm breaks down just like before.

The algorithm can be further improved by orthogonalizing the vectors of V and W. IRKA can now create the same size reduced models as IRKA with only orthogonalization. The accuracy is again the same or slightly worse than IRKA with only orthogonalization. The error and frequency response of the reduced models with size 40 and 70 are shown in Figure 4.34 for these two methods with regular

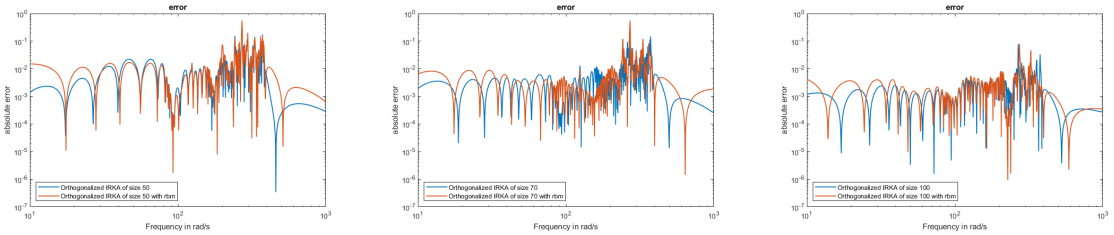

(a) Reduced model size 50

(b) Reduced model size 70

(c) Reduced model size 100

Figure 4.32: Error of IRKA using orthogonalization with and without the rigid body modes for the acoustic example

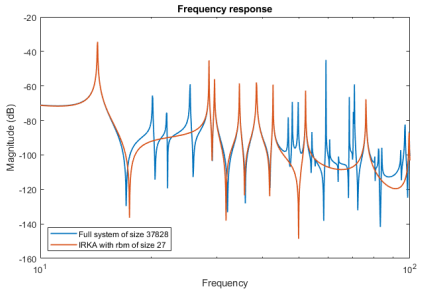

Figure 4.33: IRKA with rigid body modes for the topology optimization example

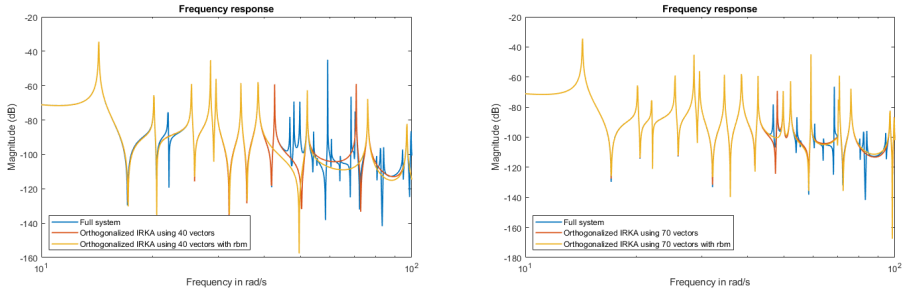

(a) Frequency response of reduced model size 40

(b) Frequency response of reduced model size 70

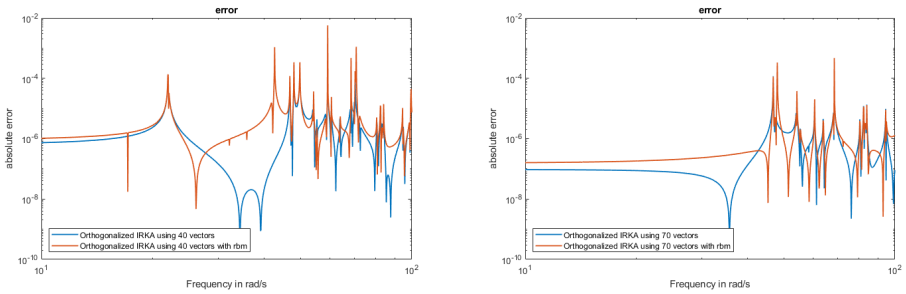

(c) Error of reduced model size 40

(d) Error of reduced model size 70

Figure 4.34: Error and FRF of IRKA using orthogonalization with and without the rigid body modes for the example of topology optimization

orthogonalization. As has been demonstrated IRKA improves when the rigid body modes are used, but a better improvement is including one of the orthogonalization method.

4.9. Two-Sided SI Arnoldi with Participation Factor vs Orthogonalized IRKA

One of the main questions of the thesis is how well do these two methods perform against each other and there are multiple strategies on how to judge this. The two main criteria will be how well the reduced models can approximate the system over the frequency domain and the number of vectors needed to match the first few peaks of the FRF.

4.9.1. Acoustic Example

IRKA with orthogonalization needs a reduced model of size 100 to visually match the FRF on the whole domain of interest. To achieve the same result with two-sided Arnoldi the reduced model needs to be of size 180. When the error plot is checked for these reduced models it shows that two-sided Arnoldi is more accurate and this level of accuracy is unattainable for IRKA. For Arnoldi of size 100 the approximation around frequency 300 is worse than IRKA, but the error for Arnoldi is still better overall. The FRF and error of these models are shown in Figure 4.35.

When the objective is to match only the first few peaks of the response function then IRKA is in-

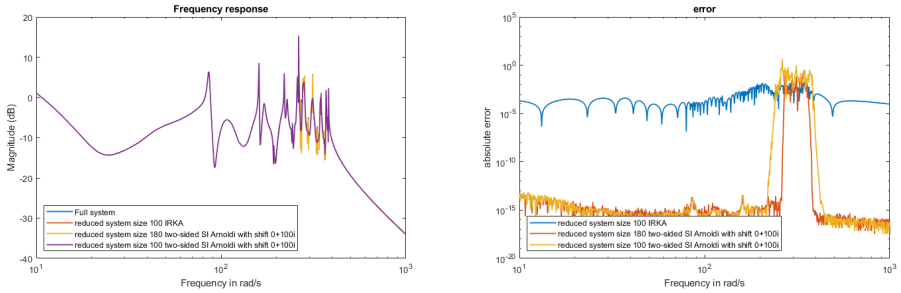

Figure 4.35: Comparison between IRKA and Arnoldi matching the full domain of interest for the acoustic example

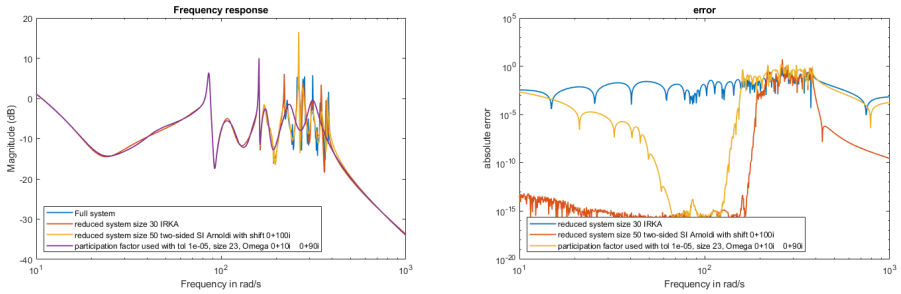

Figure 4.36: Comparison between IRKA and Arnoldi matching the start of the domain of interest for the acoustic example

herently worse than Arnoldi, since its interpolation points are spread among the whole domain. For a reduced model of size 30 it approximates the first peaks and valleys somewhat. Two-sided Arnoldi has an advantage with this, since it has one interpolation point in the middle and can reduce its size even further when combined with a participation factor. To evaluate the performance of two-sided Arnoldi we start with a reduced model of size 50 and use the transferred participation factor with the frequencies of interest as $[10\ 90]$ and a tolerance of 10^{-5}. The response function and error for both methods are shown in Figure 4.36. Again, two-sided Arnoldi performs better than IRKA.

4.9.2. Topology Optimization Example

For this example two-sided Arnoldi wins the visual approximation of the FRF. With a reduced model of 70 vectors it can fully match the frequency response function. IRKA can match most of the peaks but not all, as is shown in Figure 4.37. When the participation factor is included for two-sided Arnoldi the model reduces to size 54.

Matching the first peak for IRKA is still difficult. For a reduced model of size 50 it can match most of the peaks at the start apart from one. The reduced model of size 50 created with Arnoldi can almost match the FRF over the full domain. When the transferred participation factor is used with a tolerance of 10^{-6} and frequencies of interest $[10\ 25]$, then Arnoldi massively outperforms IRKA by creating a reduced model of size 15. This is all shown in Figure 4.38. Overall two-sided Arnoldi is a better choice for the example of topology optimization.

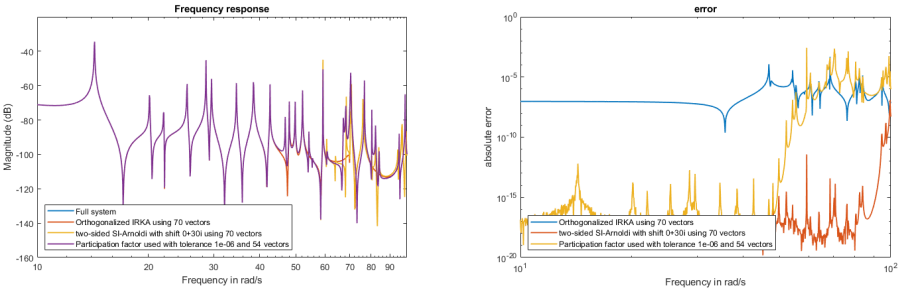

Figure 4.37: Comparison between IRKA and Arnoldi matching the start of the domain of interest for the acoustic example

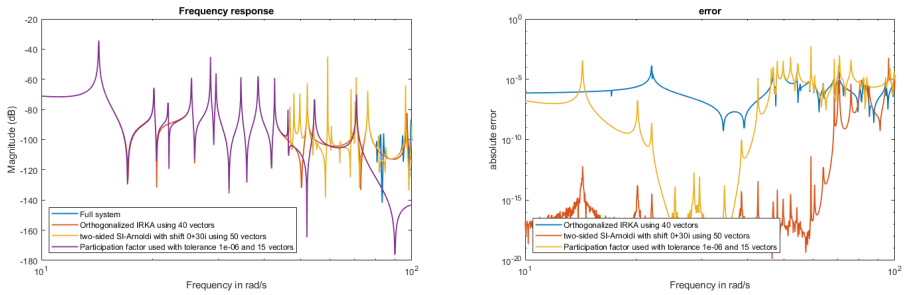

Figure 4.38: Comparison between IRKA and Arnoldi matching the start of the domain of interest for the acoustic example

5

Benchmark Problems

There exist a collection of benchmark problems for model order reduction to validate new methods and their implementation. They reflect 'real world' problems, but often cause problems for numerical methods due to ill-conditioning or near-singularity. The benchmark problems are described in [7] and can be downloaded at "http://slicot.org/20-site/126-benchmark-examples-for-model-reduction". We will discuss three of these benchmark problems to evaluate IRKA and two-sided Arnoldi. These three problems are the CD player, the Partial Element Equivalent Circuit (PEEC) model and the international space station (ISS). All of the examples are or are written to first-order linear equations. The CD player and the ISS problem have an extra complexity to them, which is having multiple input and output vectors. We will treat them as single input single output systems with some of the possible combinations for the input and output vectors.

5.1. CD Player

One of the most used examples for model order reduction is the CD player. In this example, the mechanics of a CD player are modelled with two inputs (actuation of the arm and focus of the lens) and two outputs (tracking error and focus error) [26]. The schematics of the CD player are shown in Figure 5.1.

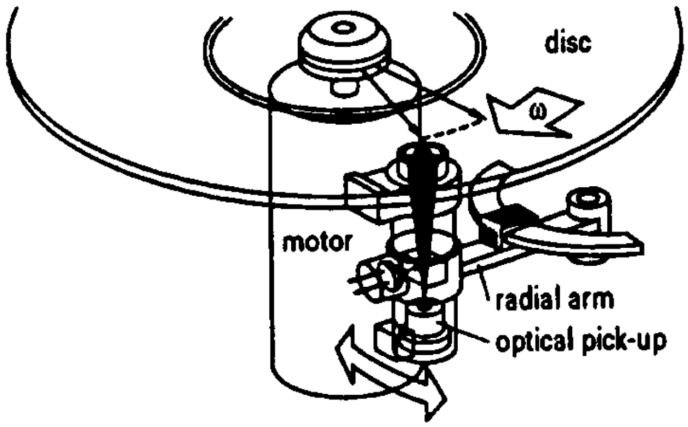

Figure 5.1: Schematics of the CD player [26]

The CD player can be described as four single input single output (SISO) system since it has two inputs and two outputs. These SISO systems are described by

$$\begin{aligned} \dot{x} &= Ax + b_i \\ y &= c_i^T x \end{aligned} \tag{5.1}$$

The systems are of size 120 and its domain of interest is $[10^{-1}\ 10^{5}]$. Many of the modifications suggested in this thesis are redundant, since $E = I$ in this example. For model order reduction we will evaluate the performance of two-sided SI Arnoldi using the preconditioner with a shift at $100i$ in combination with the participation factors and the performance of orthogonalized IRKA.

The performance is evaluated by matching the two more complex response functions of the four possible SISO systems. These are the systems combining the first input with the second output and the second input with the first output. Their response functions are shown in Figure 5.2.

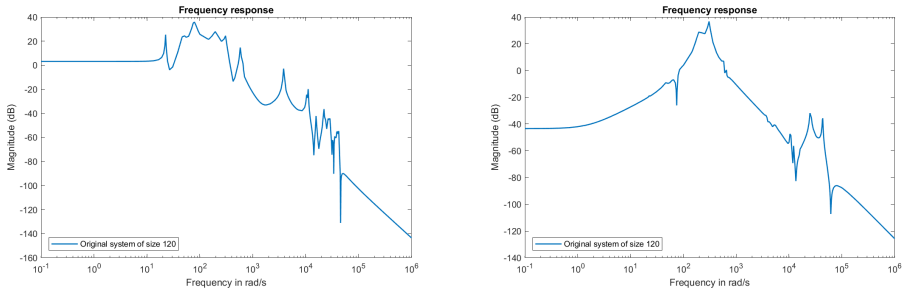

Figure 5.2: Response function of the two SISO systems for the CD player

To assess the methods we focused on visual matching the transfer functions of the reduced models with the full model. The matching for the response function using the first input and second output can be divided into three stages. Matching the response between 10^{-1} and 10^{4} and between 10^{-1} and 10^{5} and on the full domain. The size of the smallest possible models to fully match the frequency on these domains is shown in Table 5.1. From this table, we can conclude two findings. First, when you have the time to test different sizes of reduced models for Arnoldi you will find the same size model as when one of the two participation factors are used. Second, orthogonalized IRKA performs better sizewise than two-sided SI Arnoldi with all the improvements added.

For the second response function, the domain could not be divided as nicely as for the first response function, because Arnoldi would match the response at the lower frequencies for small models and IRKA would match the response at higher frequencies. The frequency domain are respectively $[10^{-1}\ 10^{4}]$ and $[10^{2}\ 10^{5}]$. For Arnoldi on the smaller domain, the smallest possible size model which matches the response function is of size 30 and is achieved without the use of a participation factor. When a participation factor is included for Arnoldi starting with a model of size 100 it creates a reduced model of size 41. The choice of participation factor does not matter in this instance. When the focus lies on matching the response function on the full domain the same results occur. This is shown in Table 5.2. When orthogonalized IRKA is used as a reduction model the reduced model size is smaller than when Arnoldi is used. This is also shown Table 5.2. Overall IRKA performs better for the CD example.

Domain	two-sided SI Arnoldi	Arnoldi size 100 with Gu	Arnoldi size 100 with the transferred	Orthogonalized IRKA
$[10^{-1}\ 10^{4}]$	40	40 (tol 10^{-5} $\Omega = 1000i$)	39 (tol 10^{-7} $\Omega = 1000i$)	30
$[10^{-1}\ 10^{5}]$	88	89 (tol 10^{-6} $\Omega = 100.000i$)	90 (tol 10^{-9} $\Omega = 100.000i$)	50
full domain	88	89 (tol 10^{-6} $\Omega = 100.000i$)	90 (tol 10^{-9} $\Omega = 100.000i$)	76

Table 5.1: Reduced models for the CD player with the first input and second output

Domain	two-sided SI Arnoldi	Arnoldi size 100 with Gu	Arnoldi size 100 with the transferred	Orthogonalized IRKA
$[10^{-1}\ 10^{4}]$	30	41 (tol 10^{-4} shift $1000i$)	41 (tol 10^{-7} shift $1000i$)	
$[10^{2}\ 10^{5}]$				20
full domain	68	73 (tol 10^{-5} shift $80.000i$)	73 (tol 10^{-8} shift $80.000i$)	35

Table 5.2: Reduced models for the CD player with the second input and first output

5.2. PEEC Model

The PEEC model is modelled after a patch antenna structure [7] and is described by

$$\begin{aligned} E\dot{x} &= Ax + b \\ y &= c^T x \end{aligned} \tag{5.2}$$

The difference between this problem and the other benchmark problems is the additional matrix E, unfortunately for this problem is the matrix very ill-conditioned. This causes the improvements related to the mass matrix to fail. The response function of this antenna on the domain $[10^{-1}\ 10^{5}]$ is shown in Figure 5.3a. IRKA could only create a reduced model which matches the transfer function at the start of the domain. For orthogonalized IRKA the largest reduced model that could be created is of size 25 and only matches the response up to frequency 4 rad/s. For bi-orthogonalized IRKA the largest reduced model is of size 70 and matches the response up to a frequency of 10 rad/s. Bi-orthogonalized IRKA is slightly better and more stable than orthogonalized IRKA. The response function is shown in Figure 5.3b. A reduced model with Arnoldi performs better than IRKA, but could not match the full response function. For a reduced model of size 40, the response function does not match between the 1 and 10 rad/s, and for a reduced model of size 120 the response function does not match for frequencies larger than 3000 rad/s. This can be seen in Figure 5.3c. Overall two-sided SI Arnoldi without mass-orthogonalization performs better than IRKA, but both are not created for a problem with an ill-conditioned E.

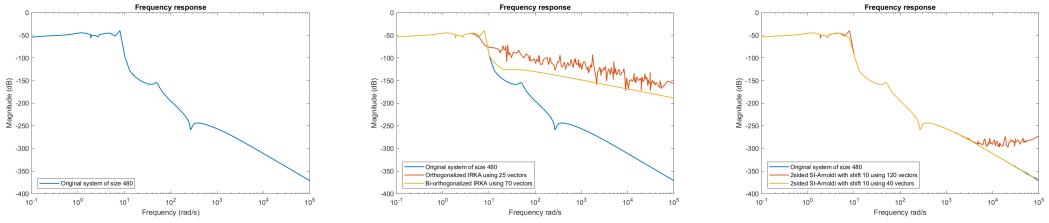

(a) Response function (b) IRKA (c) Two-sided SI Arnoldi

Figure 5.3: PEEC

5.3. International Space Station

The international space station example models the component 1r (Russian service module) of the ISS [1] and is described by the second-order system

$$M\ddot{x} + D\dot{x} + Kx = \hat{b} \tag{5.3}$$

with the assumption that M is invertible. This system is rewritten to a first-order system with the matrices

$$A = \begin{bmatrix} 0 & I \\ -M^{-1}K & -M^{-1}D \end{bmatrix} \qquad E = I$$

and the vectors

$$b = \begin{bmatrix} 0 \\ M^{-1}\hat{b} \end{bmatrix} \qquad c = b^T$$

The first-order system is of size 270 and has three inputs and three outputs. This results in 9 possible response functions. Since the response functions behave all very similar we choose one of them to evaluate the response functions of the reduced models. The response function is shown between the frequency 10^{-1} rad/s and 10^{5} rad/s. This is shown in Figure 5.4a.

The reduced model created with IRKA of size 30 can already match the response function great. It does not matter if orthogonalized IRKA or bi-orthogonalized IRKA is used. IRKA performs better than Arnoldi using a shift of $10i$ as can be seen in Figure 5.4b. The peaks and valleys around the frequency 3 rad/s are not matched when Arnoldi is used. To match these peaks Arnoldi must be of size 65. Arnoldi

is also tested in combination with the participation factor and starting with a model of size 100. Both of the participation factors find a reduced model matching all the peaks smaller than 60. This is shown in Table 5.3 together with the tolerance and omega used. The response function of the four models is shown in Figure 5.4c.

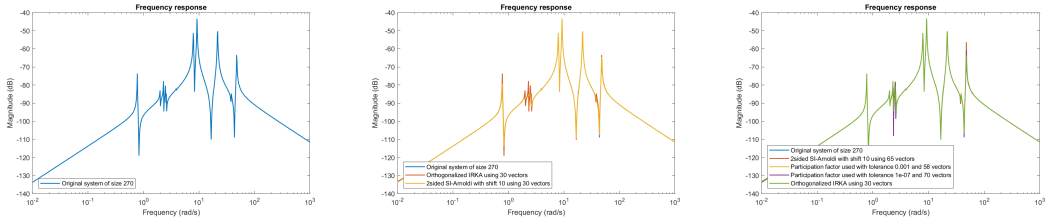

(a) Response function (b) Reduced models of size 30 (c) Response function of all methods

Figure 5.4: ISS

Domain	two-sided SI Arnoldi	Arnoldi size 100 with Gu	Arnoldi size 100 with the transferred	Orthogonalized IRKA
full domain	70	58 (tol 0.001 $\Omega = 10i$)	55 (tol 10^{-7} $\Omega = 10i$)	30

Table 5.3: Reduced models for the ISS component

6

Conclusion

The main research question of this thesis is

What is a suitable moment matching MOR method for topology optimization?

To help determine a suitable MOR method we evaluated and discussed two-sided SI Arnoldi and IRKA. For two-sided SI Arnoldi, we learned that the interpolation point should be purely imaginary and in the middle of the frequency domain. For IRKA the choice of the initial interpolation points is not relevant for its algorithm determines the location of the interpolation points by itself.

To determine the size of a reduced-order system the inclusion of the participation factor for Arnoldi is a major improvement. Although a tolerance should be guessed a priori, it will discard any vectors with a low influence on the system. Extra interest should be paid to the choice of orthogonalization of the vectors with SI Arnoldi for when the participation factor is used. In the two examples discussed the choice of orthogonalization method had no influence on the response function, but it had a big influence on the efficiency of the participation factor. when mass-orthogonalization is used for the vectors then a dot-product with respect to the mass matrix should be used in the participation factor. The same holds for the standard orthogonalization and the standard dot-product in the participation factor. For IRKA we learned that including the rigid body modes improves the reduced model to an extent, but the biggest improvement is orthogonalizing the basis created with IRKA. When IRKA with an orthogonalization method is compared with two-sided SI Arnoldi using a participation factor, one must conclude that the second is more suitable for topology optimization. One of the main reasons is the much higher accuracy of SI Arnoldi with the participations factor and the smaller models for the two evaluation examples.

For future research, the comparison between IRKA and Arnoldi can be further evaluated since with the benchmark problems IRKA was the better choice by far. A possible start for such research could lie with the rigid body modes used for IRKA. For the acoustic example, we used one rigid body mode, which was known for the second-order LTI system, but in the first-order LTI system we only had one rigid body mode for two eigenvalues equal to zero. This was the same situation for the topology optimization example where we knew three rigid body modes, but the first-order LTI system had six zero eigenvalues.

Bibliography

[1] Antoulas, A. C., Sorensen, D. C., & Gugercin, S. (2001). A survey of model reduction methods for large-scale systems. *Contemporary Mathematics, AMS Publications*, 193–219. https://doi.org/10.1090/conm/280/04630

[2] Antoulas, A. C., Beattie, C. A., & Gugercin, S. (2010). Interpolatory model reduction of large-scale dynamical systems. In J. Mohammadpour & K. M. Grigoriadis (Eds.), *Efficient modeling and control of large-scale systems* (pp. 3–58). Springer US. https://doi.org/10.1007/978-1-4419-5757-3_1

[3] Arnoldi, W. E. (1951). The principle of minimized iterations in the solution of the matrix eigenvalue problem. *Quarterly of Applied Mathematics*, *9*, 17–29. https://doi.org/10.1090/QAM/42792

[4] Bai, Z. (2002). Krylov subspace techniques for reduced-order modeling of large-scale dynamical systems [19th Dundee Biennial Conference on Numerical Analysis]. *Applied Numerical Mathematics*, *43*(1), 9–44. https://doi.org/10.1016/S0168-9274(02)00116-2

[5] Beattie, C., Drmač, Z., & Gugercin, S. (2020). Revisiting IRKA: Connections with pole placement and backward stability. *Vietnam Journal of Mathematics*, *48*(4), 963–985. https://doi.org/10.1007/s10013-020-00424-0

[6] Braun, M. (1993). *Differential equations and their applications* (Fourth Edition). https://doi.org/10.1007/978-1-4612-4360-1

[7] Chahlaoui, Y., & Van Dooren, P. (2002). A collection of benchmark examples for model reduction of linear time invariant dynamical systems. *SLICOT Working Note 2002-2*.

[8] Feldmann, P., & Freund, R. (1995). Efficient linear circuit analysis by pade approximation via the lanczos process. *IEEE Transactions on Computer-Aided Design of Integrated Circuits and Systems*, *14*(5), 639–649. https://doi.org/10.1109/43.384428

[9] Freund, R. W. (2003). Model reduction methods based on Krylov subspaces. *Acta Numerica*, *12*, 267–319. https://doi.org/10.1017/S0962492902000120

[10] Goehrke, S. A. (2017). *Topology optimization eases additive manufacturing design — a few questions for: Frustum* [Date accessed: 22/08/2022]. https://3dprint.com/169436/a-few-questions-for-frustum/

[11] Grimme, E. J. (1997). *Krylov projection methods for model reduction* (Doctoral dissertation). http://hdl.handle.net/2142/81180

[12] Gu, J., Ma, Z.-D., & Hulbert, G. M. (2000). A new load-dependent Ritz vector method for structural dynamics analyses: Quasi-static Ritz vectors. *Finite Elements in Analysis and Design*, *36*(3), 261–278. https://doi.org/10.1016/S0168-874X(00)00036-6

[13] Gugercin, S., Antoulas, A., & Beattie, C. (2008). $\mathcal{H}_2$ model reduction for large-scale linear dynamical systems. *Siam Journal on Matrix Analysis and Applications*, *30*(2), 609–638. https://doi.org/10.1137/060666123

[14] Higham, N., Mackey, D., Tisseur, F., & Garvey, S. (2008). Scaling, sensitivity and stability in the numerical solution of quadratic eigenvalue problems. *International Journal for Numerical Methods in Engineering*, *73*. https://doi.org/10.1002/nme.2076

[15] Jia, Z., & Zhang, Y. (2002). A refined shift-and-invert arnoldi algorithm for large unsymmetric generalized eigenproblems. *Computers Mathematics with Applications*, *44*(8), 1117–1127. https://doi.org/https://doi.org/10.1016/S0898-1221(02)00220-1

[16] Li, L. (2016). *What does the complex eigen-frequency imply?* [Date accessed: 04/06/2022]. https://www.researchgate.net/post/What_does_the_complex_eigen-frequency_imply/579c08a9404854368f01bf61/citation/download

[17] Rahman, M., Uddin, M., Andallah, L., & Uddin, M. (2020). Interpolatory projection techniques for $\mathcal{H}_2$ optimal structure-preserving model order reduction of second-order systems. *Advances in Science Technology and Engineering Systems Journal*, *5*(4), 715–723. https://doi.org/10.25046/aj050485

[18] Salimbahrami, B., & Lohmann, B. (2006). Order reduction of large scale second-order systems using Krylov subspace methods. *Linear Algebra and Its Applications*, *415*(2-3), 385–405. https://doi.org/10.1016/j.laa.2004.12.013

[19] Salimbahrami, B., Lohmann, B., & Bechtold, T. (2003). Two-sided arnoldi algorithm and its application in order reduction of mems. *Proc. 4th Mathmod*. https://www.eurosim.info/fileadmin/user_upload_argesim/ARGESIM_Publications_OA/MATHMOD_Publications_OA/MATHMOD_2003_AR24/paper_fulltext/022-Text-Behnam-Salimbahrmi.pdf

[20] Shamash, Y. (1975). Linear system reduction using pade approximation to allow retention of dominant modes. *International Journal of Control*, *21*(2), 257–272. https://doi.org/10.1080/00207177508921985

[21] Sigmund, O. (2001). A 99 line topology optimization code written in matlab. *Structural and Multidisciplinary Optimization*, *21*, 120–127. https://doi.org/10.1007/s001580050176

[22] Thomas, J. (2013). *Relation eigenvalue/eigenfrequency problem* [Date accessed: 04/06/2022]. https://www.comsol.com/forum/thread/32032/Relation-EigenvalueEigenfrequency-problem

[23] van Gijzen, M. B. (1999). The parallel computation of the smallest eigenpair of an acoustic problem with damping. *International Journal for Numerical Methods in Engineering*, *45*(6), 765–777. https://doi.org/10.1002/(SICI)1097-0207(19990630)45:6<765::AID-NME607>3.0.CO;2-A

[24] Vuik, C., & Lahaye, D. J. P. (2019). *Scientific computing (course wi4201)*. Delft Institute of Applied Mathematics. https://homepage.tudelft.nl/d2b4e/wi4201/wi4201_notes.pdf

[25] Wilson, E. L., Yuan, M.-W., & Dickens, J. M. (1982). Dynamic analysis by direct superposition of Ritz vectors. *Earthquake Engineering & Structural Dynamics*, *10*(6), 813–821. https://doi.org/10.1002/eqe.4290100606

[26] Wortelboer, P. M., Steinbuch, M., & Bosgra, O. H. (1999). Iterative model and controller reduction using closed-loop balancing, with application to a compact disc mechanism. *International Journal of Robust and Nonlinear Control*, *9*(3), 123–142. https://doi.org/10.1002/(sici)1099-1239(199903)9:3<123::aid-rnc396>3.0.co;2-t

[27] Zhou, K., & Doyle, J. C. (1998). *Essentials of robust control* (Vol. 104). Prentice hall Upper Saddle River, NJ.